Cellular/Molecular

The Cytidine N-Acetyltransferase NAT10 Participates in Peripheral Nerve Injury-Induced Neuropathic Pain by Stabilizing SYT9 Expression in Primary Sensory Neurons

Ming Zhang,[1*] Kehui Yang,[1*] Qi-Hui Wang,[1*] Ling Xie,[2] Qiaoqiao Liu,[1] Runa Wei,[1] Yang Tao,[1] Hong-Li Zheng,[3] Ninghua Lin,[4] Hengjun Xu,[1] Li Yang,[1] Hongjun Wang,[1] Tingruo Zhang,[1] Zhouya Xue,[5] Jun-Li Cao,[1] and Zhiqiang Pan[1]

[1]Jiangsu Province Key Laboratory of Anesthesiology, Jiangsu Province Key Laboratory of Anesthesia and Analgesia Application Technology, National Medical Products Administration (NMPA) Key Laboratory for Research and Evaluation of Narcotic and Psychotropic Drugs, Xuzhou Medical University, Xuzhou 221004, China, [2]Department of Anesthesiology, The Obstetrics and Gynecology Hospital of Fudan University, Shanghai 200011, China, [3]Department of Pain, Shanghai Tenth People's Hospital, Tongji University, Shanghai 200072, China, [4]Department of Anesthesiology, Yantai affiliated Hospital of Binzhou Medical University, Yantai 264000, China, and [5]Department of Anesthesiology, Yancheng affiliated Hospital of Xuzhou Medical University, Yancheng 224008, China

RNA N4-acetylcytidine (ac4C) modification is increasingly recognized as an important layer of gene regulation; however, the involvement of ac4C in pain regulation has not been studied. Here, we report that N-acetyltransferase 10 protein (NAT10; the only known ac4C "writer") contributes to the induction and development of neuropathic pain in an ac4C-dependent manner. Peripheral nerve injury increases the levels of NAT10 expression and overall ac4C in injured dorsal root ganglia (DRGs). This upregulation is triggered by the activation of upstream transcription factor 1 (USF1), a transcription factor that binds to the *Nat10* promoter. Knock-down or genetic deletion of NAT10 in the DRG abolishes the gain of ac4C sites in *Syt9* mRNA and the augmentation of SYT9 protein, resulting in a marked antinociceptive effect in nerve-injured male mice. Conversely, mimicking NAT10 upregulation in the absence of injury evokes the elevation of *Syt9* ac4C and SYT9 protein and induces the genesis of neuropathic-pain-like behaviors. These findings demonstrate that USF1-governed NAT10 regulates neuropathic pain by targeting *Syt9* ac4C in peripheral nociceptive sensory neurons. Our findings establish NAT10 as a critical endogenous initiator of nociceptive behavior and a promising new target for treating neuropathic pain.

Key words: **ac4C; NAT10; neuropathic pain; SYT9; USF1**

Significance Statement

The cytidine N4-acetylcytidine (ac4C), a new epigenetic RNA modification, is crucial for the translation and stability of mRNA, but its role for chronic pain remains unclear. Here, we demonstrate that N-acetyltransferase 10 (NAT10) acts as ac4C N-acetyltransferase and plays an important role in the development and maintenance of neuropathic pain. NAT10 was upregulated via the activation of the transcription factor upstream transcription factor 1 (USF1) in the injured dorsal root ganglion (DRG) after peripheral nerve injury. Since pharmacological or genetic deleting NAT10 in the DRG attenuated the nerve injury-induced nociceptive hypersensitivities partially through suppressing *Syt9* mRNA ac4C and stabilizing SYT9 protein level, NAT10 may serve as an effective and novel therapeutic target for neuropathic pain.

Received Dec. 20, 2022; revised Feb. 23, 2023; accepted Mar. 1, 2023.

Author contributions: M.Z., Q.-H.W., L.Y., H.W., J.-L.C., and Z.P. designed research; M.Z., K.Y., L.X., Q.L., R.W., Y.T., H.-L.Z., N.L., H.X., and T.Z. performed research; M.Z., Q.-H.W., L.Y., H.W., Z.X., and Z.P. analyzed data; M.Z. wrote the first draft of the paper; M.Z. and Z.P. edited the paper; M.Z. and Z.P. wrote the paper.

This work was supported by grants from the National Natural Science Foundation of China (82171234, 81971041, 81671096 to Z.P.; 82201391 to Q.-H.W.; 32200818 to L.Y.; 82171233 to H.W. and 81901132 to Z.X.); Jiang Su-Specially Appointed Professor Project; the Natural Science Foundation of Jiangsu Province Grant BK20201460; the Natural Science Foundation of Jiangsu Education Department Key Project 22KJA320008; and the Postgraduate Research and Practice Innovation Program of Jiangsu Province Grant KYCX21_2707.

*M.Z., K.Y., and Q.-H.W. contributed equally to this work.

The authors declare no competing financial interests.

Correspondence should be addressed to Zhiqiang Pan at zhiqiangp2002@aliyun.com.

https://doi.org/10.1523/JNEUROSCI.2321-22.2023

Introduction

Neuropathic pain is a major public health-care problem: it places a significant financial burden on society and often leads to emotional difficulties and problems with medication addiction in patients (Pasero, 2004; van Hecke et al., 2014). Neuropathic pain is characterized by abnormal hypersensitivity to noxious stimuli (hyperalgesia) and nociceptive responses to non-noxious stimuli (allodynia). The prevalence of neuropathic pain in the general population is estimated to range from 3% to 17% (Cavalli et al., 2019). Most of the treatments available for neuropathic pain have

side effects and only moderate efficacy, thus limiting their use. Identifying the precise mechanisms underlying neuropathic pain is essential for the discovery of novel therapeutic approaches for this disorder. Nerve-injury-induced aberrant transcriptional and translational changes in ion channels, enzymes, and cytokines/chemokines in the dorsal root ganglia (DRGs) contribute to the genesis of neuropathic pain (Alsaloum and Waxman, 2022). However, the cause of these dysfunctional changes remains unclear (J.Y. Zhao et al., 2017).

RNA modifications are emerging as an important component of posttranscriptional control over gene expression (Mongelli et al., 2020; Teng et al., 2021), and they are known to modulate neuropathic pain (Pan et al., 2021b). Recently, N4-acetylcytidine (ac4C) has been identified as an mRNA modification. It is highly conserved among all domains of life and widely distributed in human cells (Jin et al., 2020). ac4C is able to regulate mRNA stability, processing, and translation (Arango et al., 2022), and is a key determinant of posttranscriptional regulation (Arango et al., 2018). N-acetyltransferase 10 (NAT10) is the only known "writer" enzyme responsible for ac4C production in mammals (Arango et al., 2018). NAT10 overexpression deposits ac4C in sequence motifs in mRNA; NAT10 downregulation significantly decreases ac4C levels in HeLa cells (Arango et al., 2018) and, in bladder cancer cells, triggers impairments in the translation efficiency of BCL9L, SOX4, and AKT1 and inhibition of cell proliferation and migration (G. Wang et al., 2022a). NAT10-mediated ac4C modification may serve as an effective therapeutic target in disease. NAT10 is associated with many diseases, including Hutchinson–Gilford progeria syndrome (Larrieu et al., 2014), acute myeloid leukemia (Liang et al., 2020), several cancers (Tan et al., 2013; H. Zhang et al., 2014; Tschida et al., 2017; Y. Zhang et al., 2021), anxiety, and depression (Guo et al., 2022). Nevertheless, it remains to be determined whether NAT10 participates in the regulation of neuropathic pain through modulation of ac4C.

The synaptotagmin (SYT) protein family is responsible for Ca^{2+} sensing in synaptic vesicles and regulates exocytosis by fine-tuning Ca^{2+}-dependent neurotransmitter release from presynaptic terminals (Geppert et al., 1994; Fernandez-Chacon et al., 2001). The SYT family has 17 members, with SYT1 and SYT2 already known to be involved in the development and maintenance of pain. For example, SYT1 siRNA knockdown or antibody blockade attenuates nerve-injury-induced neuropathic pain (Alvarado et al., 2015; Wan et al., 2020). SYT9 is reported to participate in neuronal differentiation (Y. Wang et al., 2016), cancer development (Bao et al., 2011; Yang et al., 2021), and Alzheimer's disease (Gautam et al., 2015), but whether *Syt9* is also associated with neuropathic pain remains to be elucidated.

Here, we report that chronic constriction injury (CCI) of peripheral nerves, a model of neuropathic pain that mimics clinical symptoms, led to increases in global RNA ac4C and NAT10 in mouse DRG. In this study, we found the nerve injury-induced increase of SYT9 protein was blocked by the knock-down of *Nat10* in mice DRG. CCI also induced an increase in SYT9 protein in the DRG, which was blocked by knock-down of NAT10. These results suggest that NAT10 downregulation is required for the initiation and maintenance of CCI-induced neuropathic pain through ac4C-controlled translation of SYT9. NAT10-mediated ac4C RNA modification is likely a critical epigenetic player in nerve-injury-induced pain hypersensitivity, an insight that may provide a new understanding of the mechanisms underlying neuropathic pain.

Materials and Methods

Animals

Two mouse strains, BALB/C mice from Xuzhou Medical University and $Nat10^{fl/fl}$ mice purchased from Cyagen Biosciences, were used in this study. Pups were kept with their female parent after born and weaned at postnatal day 21, then group housed by sex with four to five mice per cage. Mice were housed with littermates (less than five in a vivarium) in temperature-controlled rooms on a 12/12 h light/dark cycle. Food and water were provided *ad libitum*. Male mice were age-matched, and used at 8–10 weeks of age. The conditional knock-out (cKO) mice lacking *Nat10* in DRG were generated by microinjected rAAV-hSyn-*Cre* virus into unilateral lumbar (L)3/4 DRGs. *Nat10* conditional knock-out mice were viable and did not exhibit visible abnormalities. All procedures were performed according to the guidelines of the Animal Care and Use Committee of Xuzhou Medical University.

Mouse genotyping

$Nat10^{fl/fl}$ cKO mice were identified by genotyping. DNA was extracted from clipped tail of mice and extracted in 50 μl of DNA lysis buffer containing proteinase K by incubation in 55°C for 4–6 h. Then, TE buffer was added at 95°C for inactivate proteinase K. The mice genotype was identified by using PCR primers in Table 1. The homozygotes were one band with 204 bp, heterozygotes two bands with 204 and 133 bp, and wild type (WT) one band with 133 bp (Extended Data Fig. 3-1*i*,*j*).

Animal models

For neuropathic pain models, sciatic nerve chronic constriction injury (CCI), spinal nerve ligation (SNL), and spared nerve injury (SNI) model were performed as published previously (Rigaud et al., 2008; X. Zhao et al., 2013; Y. Wang et al., 2020). Briefly, mice were placed under anesthesia with 1% pentobarbital sodium. For CCI model, left sciatic nerve was exposed and loosely ligated with 4–0 silk thread at three sites with an interval of ~1 mm proximal to trifurcation of the sciatic nerve. For SNL neuropathic pain model, the underlying spinal nerve L4 was isolated and ligated with 7–0 silk thread. The ligated nerve was then transected distal to the ligature. For SNI, a small incision was made at the lateral skin of the thigh to exposed the sciatic nerve and its three branches: the sural, common peroneal, and tibial nerves. The tibial and common peroneal nerves were carefully ligated and transected and the intact sural nerve was preserved. The wound of those model was closed with 6–0 silk sutures to the muscles and 5–0 silk sutures to the skin. Sham animals received an identical surgery but without the ligation or transection of the respective nerve.

DRG microinjection

DRG microinjection was conducted as described previously to deliver the siRNA or virus (Y. Li et al., 2020; Pan et al., 2021b). In brief, unilateral L3 and L4 DRGs were exposed. The viral solution (1 μl/DRG, 4×10^{12} GC/ml for rAAV; 10^8 TU/ml for lentivirus) or siRNA solution (1 μl/DRG, 40 μM) was injected into unilateral exposed L3/4 DRGs with the use of a glass micropipette connected to a Hamilton syringe at the rate of 20 μl h^{-1}. The glass electrode was left in place for 5 min after the injection. Animals showing signs of paresis or other abnormalities were excluded after DRG microinjection. All the siRNA were verified *in vivo* and *in vitro* by quantitative real-time polymerase chain reaction (qRT-PCR), the sequence of siRNA in this study are all in Table 1.

Behavioral tests

Mechanical, heat, and locomotor function tests were conducted as described (Y. Li et al., 2020; Pan et al., 2021b). The mechanical and heat stimuli response was performed in sequential order at 1-h intervals, locomotor function test before all behavioral tests.

Paw-withdrawal frequency (PWF) in response to mechanical stimuli were measured with two calibrated von Frey filaments as previous described (0.07 and 0.4 g, Stoelting Co; Y. Li et al., 2020; Pan et al., 2021b). Briefly, mice were placed in a plastic cage with a metal mesh floor and habituated 30 min before test. Two calibrated von Frey filaments were used to stimulate the hind paw for approximately 1 s, and each stimulation was repeated 10 times to both hind paws with a 5-min

interval. A quick withdrawal of paw was regarded as a positive response. The number of positive responses among 10 applications was recorded as percentage withdrawal frequency [(number of paw withdrawals/10 trials) × 100 = % response frequency].

Thermal nociceptive behavior was assessed by measuring each mouse's paw-withdrawal latency in response to thermal stimulus with a Model 336 Analgesia Meter (IITC Inc. Life Science Instruments) as previous method (Pan et al., 2019). In brief, mice were placed in a Plexiglas chamber on a glass plate and habituated 30 min. A light beam was used for stimulating the plantar center. Paw-withdrawal latency (PWL) was recorded as the time elapsed from the start of the light beam to foot withdrawal. Each test was repeated five times at 5-min intervals, for 20-s maximum to avoid tissue injury.

Locomotor functions, including placing, grasping, and righting reflexes, were examined before the above-described behavioral tests. (1) Placing reflex: Put hindlimbs slightly lower than forelimbs, and the dorsal surfaces of the hind paws were brought into contact with the edge of a table. It was recorded if the hind paws were placed on the table surface reflexively. (2) After the animal was placed on a wire grid, it was recorded if the hind paws grasped the wire on contact. (3) Righting reflex: When the animal was placed on its back on a flat surface, it was recorded if it immediately assumed the normal upright position. Each test was repeated five times and the score of each response was recorded.

Cell line culture and transfection

HEK293T and HT22 cell were cultured in DMEM (Gibco/ThermoFisher Scientific) containing 10% v/v fetal bovine serum (FBS; Gibco/ThermoFisher Scientific) at 37°C in a humidified incubator with 5% CO_2. The plasmids, siRNAs were transfected into the cells with ExFect Transfection reagent (Vazyme) according to the manufacturer's instructions.

DRG neuronal isolated and culture

Primary DRG neurons were generated as previously described (Y. Li et al., 2020). Briefly, the DRG from three- to four-week mice was isolated and collected in cold Neurobasal Medium (Gibco/ThermoFisher Scientific) containing 10% FBS (JR Scientific), penicillin and streptomycin (C0222, Beyotime). Then the DRG was treated with collagenase Type I and trypsin-EDTA (0.25%). After trituration and centrifugation, dissociated cells were resuspended in a mixed Neurobasal Medium. Then the cells were plated on poly-D-lysine-coated (Sigma-Aldrich)-treated dishes and incubated at 37°C with 5% CO_2 and 95% air.

RNA extraction and quantitative real-time polymerase chain reaction (qRT-PCR)

Mice were anesthetized with isoflurane and the L3/4 DRGs removed rapidly on ice then stored at −80°C. Total RNA was extracted from DRG tissue with TRIzol reagent according to the instructions (R401-01, Vazyme). RNA concentration was measured using the NanoDrop 2000 Spectrophotometer (Thermo Scientific); 400 ng total RNA were reverse-transcribed into cDNA using reverse transcriptase M-MLV (2641A; Takara). Then the cDNA was used for template for real-time quantitative PCR with corresponding primers in Table 1. Each sample was run in triplicate in a 10-µl reaction using SYBR Premix ExTaqII (RR820A; Takara). Reactions were conducted in a Roche Light Cycler 480 system. The expression levels of the target genes were quantified relative to glyceraldehyde-3-phosphate dehydrogenase (Gapdh) expression (cycle threshold; CT) using the $2^{-\Delta\Delta CT}$ method as described previously (Pan et al., 2019).

ac4C dot-blot

Total ac4C dot-blot analysis was performed as described previously (Arango et al., 2018). Briefly, 500 ng of RNA were denatured at 75°C for 5 min, immediately placed on ice for 1 min and loaded onto Hybond-N^+ membranes and then crosslinked with UV254 for 10 min. Blocked with 5% nonfat milk for 2 h at room temperature (RT), and incubated with the antibody specific to ac4C (1:1000; A18806, ABclonal) at 4°C overnight. After 0.05% Tween 20 PBS (PBST) washed three times, horseradish peroxidase-conjugated rabbit IgG antibody was incubated 2 h at RT. The signal was visualized by using ECL (P0018S, Beyotime). Equal RNA loading was verified by staining the membranes with 0.2% methylene blue. The intensity of each dot was normalized to total RNA.

Plasmid constructs and virus production

Full-length of *Usf1*, *Nat10*, and *Syt9* was, respectively, amplified from mouse cDNA. The lentivirus proviral plasmids treated with BamHI and then ligated the PCR product into the BamHI site with ClonExpress II One Step Cloning kit (C112, Vazyme). For Lenti-shRNA, synthesized LV-Nat10-shF and LV-Nat10-shR oligos were annealed and then ligated to the lentivirus vector pLVTHM which had been treated with MluI and ClaI. Primers and oligos sequence are all in Table 1. All constructed plasmids were confirmed by Sanger's sequencing. The lentivirus package and production were performed as described previously (Pan et al., 2016). The constructed core plasmid (8 µg) and two envelope plasmids, PSPAX2 (6 µg) and PMD2G (2 µg), were co-transfected into HEK293T cells in a 10 cm dish according to manufacturer instructions of ExFect Transfection reagent (Vazyme). The supernatant was collected at 48 h after transfection, and concentrated by using a Centricon Plus-70 filter unit (UFC910096, Millipore).

Tandem mass tags (TMT) proteomics analysis

TMT proteomics analysis was performed as described previously (Friedrich et al., 2021). Briefly, sample was added SDT buffer and homogenized in 2-ml tubes. The homogenate was sonicated and then boiled for 15 min. After centrifuged at 14,000 × *g* for 40 min, the supernatant was filtered with 0.22 µm filters. The filtrate was quantified with the BCA method. Next, 200 μg of proteins for each sample were treated with FASP Digestion and then labeled using TMT reagent according to the manufacturer's instructions (90113CH, ThermoFisher Scientific). TMT-labeled peptides were fractionated by RP chromatography using the Agilent 1260 infinity II HPLC and then analyzed by mass spectrometry. MS/MS raw files were processed using MASCOT engine (Matrix Science; version 2.6) embedded into Proteome Discoverer 2.2, and searched against the Uniprot-MusMusculus-17056-20210125 database. Proteins with fold change >1.2 and *p*-value (Student's *t* test) < 0.05 were considered to be differentially expressed proteins.

CRISPR vector of specifically targeting ac4C site in Syt9 *CDS*

The dCasRx and NAT10 fusion vector construction in Lenti-CRISPR was conducted as the previously described with few modifications (J. Li et al., 2020). Briefly, full-length of *Nat10* was amplified from mouse cDNA and then ligated into the BamHI treated EF1a-dCasRx-2A-EGFP vector with ClonExpress II One Step Cloning kit (C112, Vazyme). Lentivirus gRNA including gRNA-27 (targeting +27 to +46 of Syt9 CDS, first nucleotide in CDS designated as +1) and gRNA-153 (targeting +153 to +172) and negative control gRNA were constructed through ligating to pLH-sgRNA1 according to the previous report (Ma et al., 2016). In brief, forward and reverse oligos (Table 1) were annealed and ligated to single BbsI-digested pLH-sgRNA1 vectors. The lentivirus package and titer identification were seen in the above described in Plasmid Constructs and Virus Production part. Lentivirus-dCasRx-NAT10 and Lenti-gRNA were co-microinjection into L3/4 DRGs and then used in the experiment after the identification of their effect.

Western blotting

To achieve sufficient protein, two unilateral mouse DRG were pooled together. After washed three times in precold PBS, DRG were homogenized in RIPA buffer (P0013B, Beyotime). After centrifugation at 4°C for 15 min at 12,000 rpm, the supernatant was collected and then used the BCA kit (P0012S, Beyotime) to measure the sample concentration. Total 20–40 µg of protein were electrophoresed by Bio-Rad protein system (Bio-Rad Laboratories). The proteins were then electrophoretically transferred onto a polyvinylidene difluoride membrane (IPVH85R, Millipore). After the membranes were blocked with 3% nonfat milk in Tris-buffered saline containing 0.1% Tween 20 for 1 h, they were incubated overnight at 4°C with the following primary antibodies including NAT10 (1:1000, ET7111-23, HUABIO), SYT9 (1:1000, ER61289, HUABIO), upstream transcription factor 1 (USF1; 1:1000, BS6759, Bioworld), p-ERK 1/2 (1:1000, 28 733–1-AP, Proteintech),

Table 1. The primer used in this experiment

Name	Sequences
RT-qPCR	
Nat10F	GCGGCAGAGGTCTCTTTTTGT
Nat10R	GTGACTGCTAAATCCCAGCTC
Syt9F	CTGCCAAGATTTCATCTACCACC
Syt9R	TCCAAGACACGAAAAGAGAGACA
Usf1F	CTGAAACCGAAGAGGGAACAG
Usf1R	GTTGGGGTCAGGAAAAGTGG
GAPDH-F	GGTGAAGGTCGGTGTGAACG
GAPDH-R	CTCGCTCCTGGAAGATGGTG
Cloning	
PCD-Nat10F	AATTCGAATTTAAATCGGATCCATGAATCGGAAGAAGGTGGATAA
PCD-Nat10R	GATCCTTGCGGCCGCGGATCCCTACTTCTTTCGCTTCAGTTTCA
Nat10-shRNAF	CGCGTTTGCCCAGAATCTTGTGGGTTCAAGAGACCCACAAGATTC TGGGCAATTTTTGGAAAT
Nat10-shRNAR	CGATTTCCAAAAATTGCCCAGAATCTTGTGGGTCTCTTGAACCCAC AAGATTCTGGGCAAA
PCD-Syt9F	AATTCGAATTTAAATCGGATCCATGCCCGGGGCCAGGGACGCGCT
PCD-Syt9R	GATCCTTGCGGCCGCGGATCCTCATCGTTTCTCCATCAGAGAG
PCD-Usf1F	AATTCGAATTTAAATCGGATCCATGAAGGGGCAGCAGAAAACAG
PCD-Usf1R	GATCCTTGCGGCCGCGGATCCTTAGTTGCTGTCATTCTTGATG
dCasR-Nat10F	GTGTCCGGCAATTCCGGATCCATGAATCGGAAGAAGGTGGATAA
dCasR-Nat10R	CTTTTTCTTAGGTCCGGATCCCTACTTCTTTCGCTTCAGTTTCA
gR-Sy9-27F	ACCGTCACCAGGCGCTGCAGCTGC
gR-Sy9-27R	AAACGCAGCTGCAGCGCCTGGTGA
gR-Sy9-153F	ACCGTGTGAGCCTGCTAACCCTCG
gR-Sy9-153R	AAACCGAGGGTTAGCAGGCTCACA
gR-ScrF	ACCGTTCTCCGAACGTGTCACGT
gR-ScrR	AAACACGTGACACGTTCGGAGAA
pGL6-Nat10F	GCCGGTACCGCTAGCCTCGAG TCAGTCCAACTACTTGATAGG
pGL6-Nat10R1	TCTACGCGTGAGCTCCTCGAGAGCACGTGGGCAAGTGCTC
pGL6-Nat10R2	TCTACGCGTGAGCTCCTCGAGGCTACCCAGGCTGACCAATC
siRNA	
Scramble-S	UUCUCCGAACGUGUCACGUTT
Scramble-AS	ACGUGACACGUUCGGAGAATT
Nat10-566-S	CCCACAAGAUUCUGGGCAATT
Nat10-566-AS	UUGCCCAGAAUCUUGUGGGTT
Nat10-1138-S	GCAGUGGCAUUCGGGUAUUTT
Nat10-1138-AS	AAUACCCGAAUGCCACUGCTT
Syt9-287-S	UGGAGCACGACAGCUGCCAAGAUUUTT
Syt9-287-AS	AAAUCUUGGCAGCUGUCGUGCUCCATT
Syt9-735-S	CAACCUGUCGAACCCGGACUUUAAUTT
Syt9-735-AS	AUUAAAGUCCGGGUUCGACAGGUUGTT
Usf1-316-S	AGCAUCCAGUCAGCUGCCACUTT
Usf1-316-AS	AGUGGCAGCUGACUGGAUGCUTT
Usf1-395-S	ACAGGGUGAUCCAGGUGUCATT
Usf1-395-AS	UGACACCUGGAUCACCCUGUTT
RIP-PCR	
RIP-S9-F1	TGGAGCACGACAGCTGCC
RIP-S9-R1	GGCAGTAACCACGAGGGTTA
RIP-S9-F2	GTGGACCACTTCTTCGACT
RIP-S9-*R*2	CATTATCGTTGGTGACATACT
RIP-S9-F3	AGTATGTCACCAACGATAATG
RIP-S9-R3	TCACGTAGGGATCTGATGCT
RIP-S9-F4	GTTTACAATGAAGCCATAGT
RIP-S9-R4	CACGGTCATAGTCCATGAC
ChIP-PCR	
ChIP-1F	TCAGTCCAACTACTTGATAGG
ChIP-1R	TGGCTGAGCTGTCTATGCTG
ChIP-2F	CAGCATAGACAGCTCAGCCA
ChIP-2R	TGGCTATGATTACCTTAGTCAC
ChIP-3F	ATATGGCTAGGCATCATGAAG
ChIP-3R	TGAGCCACGTGAAATCGGTTT
ChIP-4F	TAAACCGATTTCACGTGGCTCA
ChIP-4R	CTTACTCATGCCAAGTGTACTA

(*Table continues.*)

Table 1. Continued

Name	Sequences
Single-cell PCR	
Usf1-outF	CTGAAACCGAAGAGGGAACAG
Usf1-outR	GTGGCAGGGTAACCACTGATG
Nat10-outF	TCATTGAGAATGGCGTAGCTG
Nat10-outR	GTGACTGCTAAATCCCAGCTC
Syt9-outF	CTGCCAAGATTTCATCTACCACC
Syt9-outR	ACAGTTTCCAAGACACGAAAAGA
NeuN-outF	AGACAGACAACCAGCAACTC
NeuN-outR	CTGTTCCTACCACAGGGTTTAG
GAPDH-outF	AGGTTCATCAGGTAAACTCAG
GAPDH-outR	ACCAGTAGACTCCACGACAT
Usf1-inF	AGGACCCAACTAGTGTAGC
Usf1-inR	GTTGGGGTCAGGAAAAGTGG
Nat10-inF	GCGGCAGAGGTCTCTTTTTGT
Nat10-inR	CACAGTTGCCTTGGACAACAT
Syt9-inF	TGTGAGCCTGCTAACCCTC
Syt9-inR	TCCAAGACACGAAAAGAGAGACA
NeuN-inF	ACGATCGTAGAGGGACG
NeuN-inR	TTGGCATATGGGTTCCCAGG
GAPDH-inF	ACCAGGGCTGCCATTTGCA
GAPDH-inR	CTCGCTCCTGGAAGATGGTG

ERK1/2 (1:1000, 11257-1-AP, Proteintech), β-Tubulin (1:2000, 10068-1-AP, Proteintech), and GAPDH (1:2000, ET1601-4, HUABIO). The membranes were then washed twice in tris-buffered saline with Tween 20 at room temperature for 10 min. Next, incubated with anti-rabbit IgG secondary antibodies (1:2000, A0208, Beyotime) 2 h at room temperature. After washed three times, visualized by ECL reagent (P0018FS, Beyotime) and exposed using the UVITEC System (Q9 Alliance, UVITEC). The specificity of NAT10, USF1, and SYT9 antibodies were verified (Extended Data Figs. 2-1*b*, 3–1*e*, and 6–1*b*) by using Western blotting at 48 h after transfection of their individual siRNA in the cultured DRG neurons as described previously (J.Y. Zhao et al., 2021). All protein bands were normalized to GAPDH or Tubulin.

Measurement of newly synthesized protein

Measurement of global protein synthesis was described previously (Schmidt et al., 2009; Pan et al., 2021a). In brief, puromycin (10 mg/kg) were intraperitoneally injected 1 h before DRG tissues collection for Western blotting. Thirty micrograms of total protein were separated by 10% SDS-PAGE and transferred onto PVDF membranes. After blocked with 5% no-fat milk, mouse anti-puromycin antibody (1:1000; MABE343, Millipore) was incubated overnight at 4°C. HRP-labeled Goat Anti-mouse IgG (1:2000; A0216, Beyotime) was then applied at room temperature for 1.5 h. Last, the membranes visualized by ECL reagent (P0018FS, Beyotime) and exposed using the UVITEC System (Q9 Alliance, UVITEC). Membranes were washed by stripping buffer and incubated with rabbit anti-GAPDH antibodies (1:2000, ET1601-4, HUABIO) followed by HRP-labeled Goat Anti-rabbit IgG (1:2000; A0208, Beyotime) as the loading control. Newly synthesized protein was quantified by detecting immune complexes signal intensities approximately ranged from 15 to 180 KD. Band intensities of the target signals normalized to those of GAPDH for statistical analyses.

Immunohistochemistry

The procedure was performed as previous described (Pan et al., 2021b). Briefly, Animals were anesthetized with pentobarbital sodium and perfused with 4% paraformaldehyde. The L3 and L4 DRGs were collected, postfixed, dehydrated in 30% sucrose, and dehydrated before frozen sectioning at 15 μm. The sections were blocked with 10% goat serum and 0.4% Triton X-100 in 0.01 M PBS at room temperature for 1 h and then incubated with the following primary antibodies over one or two nights at 4°C. The antibodies and regents include: NAT10 (1:200, ET7111-23, HUABIO), NAT10 (1:100, sc-271770, Santa Cruz), CGRP (1:50, SC57053, Santa Cruz), IB4 (1:200, L9381, Sigma), NF200 (1:200, 60331-1-lg, Proteintech), β-Tubulin III (1:500, M0805-8, HUABIO), Glutamine Synthesis (1:500, EM1902-39,

HUABIO), SYT9 (1:200, GTX45560, GeneTex), and USF1 (1:100, BS6759, Bioworld). The sections were then incubated with corresponding fluorescent-conjugated secondary antibody (A32766, A32744, A32790, A32754, Invitrogen) 1 h at room temperature. After 0.4% Triton X-100 buffer washed three times, the sections finally were mounted on a mounting medium with DAPI and examined using an Olympus FV1000 laser confocal microscope.

Chromatin immunoprecipitation (ChIP)

The ChIP assay was conducted using a ChIP Assay kit (P2078, Beyotime). To achieve sufficient DNA, four unilateral mouse L3/4 DRGs were pooled together. The homogenate from the DRG was crosslinked with 1% formaldehyde at room temperature for 10 min. The reaction was stopped by the addition of glycine (0.25 M). After the DNA sonicated into fragments with a mean length of 200–1000 bp, Protein A+G Agarose/Salmon Sperm DNA was added to reduced nonspecific binding. Then the USF1 (1 μg, sc-390027, Santa Cruz) primary antibody or purified mouse IgG overnight at 4°C. Input (20% of the sample for immunoprecipitation) was used as a positive control. The DNA fragments were purified and identified using PCR/real-time PCR with the primers listed in Table 1.

RNA immunoprecipitation assay (RIP)

The RNA immunoprecipitation (RIP) assay was conducted as the Abcam protocol with minor modification. Briefly, the homogenates from DRG were suspended in the RIP lysis buffer containing protease inhibitor cocktail (VPI012, VICMED) and RNase inhibitor (RK21401, ABclonal). Rabbit anti-ac4C antibody (1 μg, ab252215, Abcam) or normal rabbit IgG (1 μg, A7016, Beyotime) were added to corresponding sample overnight at 4°C by rotating. Then, Protein A+G Agarose (P2055, Beyotime) were added to conjugated the antibody at 4°C for 1 h. After the samples were washed three times with the RIP wash buffer, RNA was eluted with TE buffer and extracted by TRIzol (R401-01, Vazyme). The qPCR was performed after reverse transcription and the primers listed in Table 1.

Polyribosome fractionation assay

According to the previously described with few modifications (Panda et al., 2017; Pan et al., 2021a). Briefly, five different sucrose gradient solutions (7%, 17%, 27%, 37%, and 47% in Tris-HCl) were added into a 10.4 ml tube (Beckman, 355603) gently. Each gradient was 2 ml with a progressively decreasing sucrose concentration from the bottom of the tube. After washing three times with ice-cold 1× PBS, DRG tissues from eight mice were digested in freshly prepared lysis buffer. Tissues were mechanically sheared using a homogenizer and centrifuged, and 400 μl of supernatant were added on the top of the tube. After centrifugation (36,000 rpm for 2 h at 4°C with max break), solutions in the tube were split into 15 equal fractions. Each fraction was extracted total RNA with 1.5 ml TRIzol (R401-01, Vazyme) for *Syt9* mRNA qRT-PCR.

Luciferase assay

The 1249-bp fragment from the *Nat10* gene promotor region (including USF1-binding motif) was amplified by PCR from genomic DNA with the primers (Table 1) to construct the *Nat10* gene reporter plasmid. The PCR products were ligated into the XhoI restriction sites of the pGL6-Basic vector with ClonExpress II One Step Cloning kit (C112, Vazyme). The accuracy of recombinant clones was verified by DNA sequencing. HEK-293T cells were plated on a 24-well plate and cultured at 37°C in a humidified incubator with 5% CO_2. One day after culture in which the cell density was ~50–60%, the cells in each well were co-transfected with 200 ng of a plasmid expressing full-length *Usf1*, 200 ng of pGL6-Basic vector with or without the *Nat10* promoter sequence, and ExFect Transfection reagent (Vazyme), according to the manufacturer's instructions. Two days after transfection, cells were collected and lysed by Dual Luciferase Reporter Gene Assay kit (RG027, Beyotime). Approximately 100 μl of supernatant was used to measure the luciferase activity using the Dual Luciferase Reporter Assay System (Promega). The relative reporter activity was calculated after normalization by the coelenterazine activity to *Renilla* activity.

Experimental design and statistical analysis

Statistical analysis was performed by GraphPad 8.0 as described previously (Pan et al., 2021a, b). The size of the experimental groups was determined based on the literature of the field and our previous experience (Pan et al., 2019; Yi et al., 2021). Each experiment presented in the study was repeated in multiple animals (four to eight mice per sample, see relevant sections). In all experiments, the relevant animals were allocated to experimental groups randomly. To specifically regulate genes expression in DRG, DRG microinjection was used here for virus or siRNA injection, as described previously (Pan et al., 2021b; Du et al., 2022). Double-blind tests were adopted in all behavioral experiments. Additionally, to exclude the effect of locomotor impairment on the pain behavior data, locomotor function was included in this study. All data were presented as mean ± SEM. Data distribution was assumed to be normal but this was not formally tested. The data were statistically analyzed using two-tailed, unpaired Student's *t* test, and one-way or two-way ANOVA. When ANOVA showed a significant difference, a pairwise comparison between means was performed using the *post hoc* Tukey's method; $p<0.05$ was considered statistically significance in all analyses.

Results

Peripheral nerve injury increases the level of ac4C and NAT10 expression in the DRG

To investigate the role of ac4C modification in nociceptive behavior, we first examined changes in the global level of ac4C in the ipsilateral lumbar 3 and 4 (L3/4) DRGs after CCI in mice. Dot-blot results show that DRG ac4C increased in a time-dependent manner after CCI surgery (Fig. 1*a*). There were no differences between the CCI group and the sham group for the first 3 d after surgery, but the level of ac4C was significantly higher in the CCI group at the 7- and 14-d time points (Fig. 1*a*). Given the existence of positive correlations in epigenetic markers in the urine, blood, and CSF under disease conditions (Parsons et al., 2014; Liu et al., 2021; Ye et al., 2021), we also evaluated changes in RNA ac4C in blood drawn from the periphery. As expected, there was a global increase in ac4C in blood taken from CCI mice (Extended Data Fig. 1-1*a*). These data suggest that the blood ac4C level may reflect the changes in DRG ac4C levels with neuropathic pain.

NAT10 is the only protein known to transfer an N4-acetyl group to cytosine in the RNA; thus, we hypothesized that nerve injury may alter the expression of NAT10 in the DRG. Relative to the sham group, Nat10 mRNA was increased by 184% and 178% on days 7 and 14, respectively, in ipsilateral L3/4 DRGs after unilateral CCI surgery, but no significant increases were seen on days 1 and 3 (Fig. 1*b*). Nat10 mRNA was not altered in contralateral L3/4 DRGs after CCI (Extended Data Fig. 1-1*b*). Similarly, the level of NAT10 protein in the ipsilateral L3/4 DRGs was significantly enhanced on days 7 and 14, but not days 0–3, after CCI injury (Fig. 1*c*), but not after sham surgery. To further confirm this result, we measured NAT10 protein expression in the DRG with two other neuropathic pain models, spinal nerve ligation (SNL) and spared nerve injury (SNI). Consistent with the CCI results, NAT10 was increased in the ipsilateral DRG in SNL mice by 78% on day 7 and 130% on day 14, but was not increased on days 1 and 3 (Fig. 1*d*). Interestingly, NAT10 was increased only on day 7 with the SNI model (Fig. 1*e*). To test whether DRG NAT10 is affected by inflammatory nociception, we injected complete Freund's adjuvant (CFA) into the plantar surface of the unilateral hind paw, a preclinical animal model of chronic inflammatory pain (Pan et al., 2017), and then measured the expression of NAT10 from 2 h to 7 d afterward. We observed a slight increase in NAT10 in L3/4 DRGs after CFA injection, but the change was not statistically significant (Extended Data

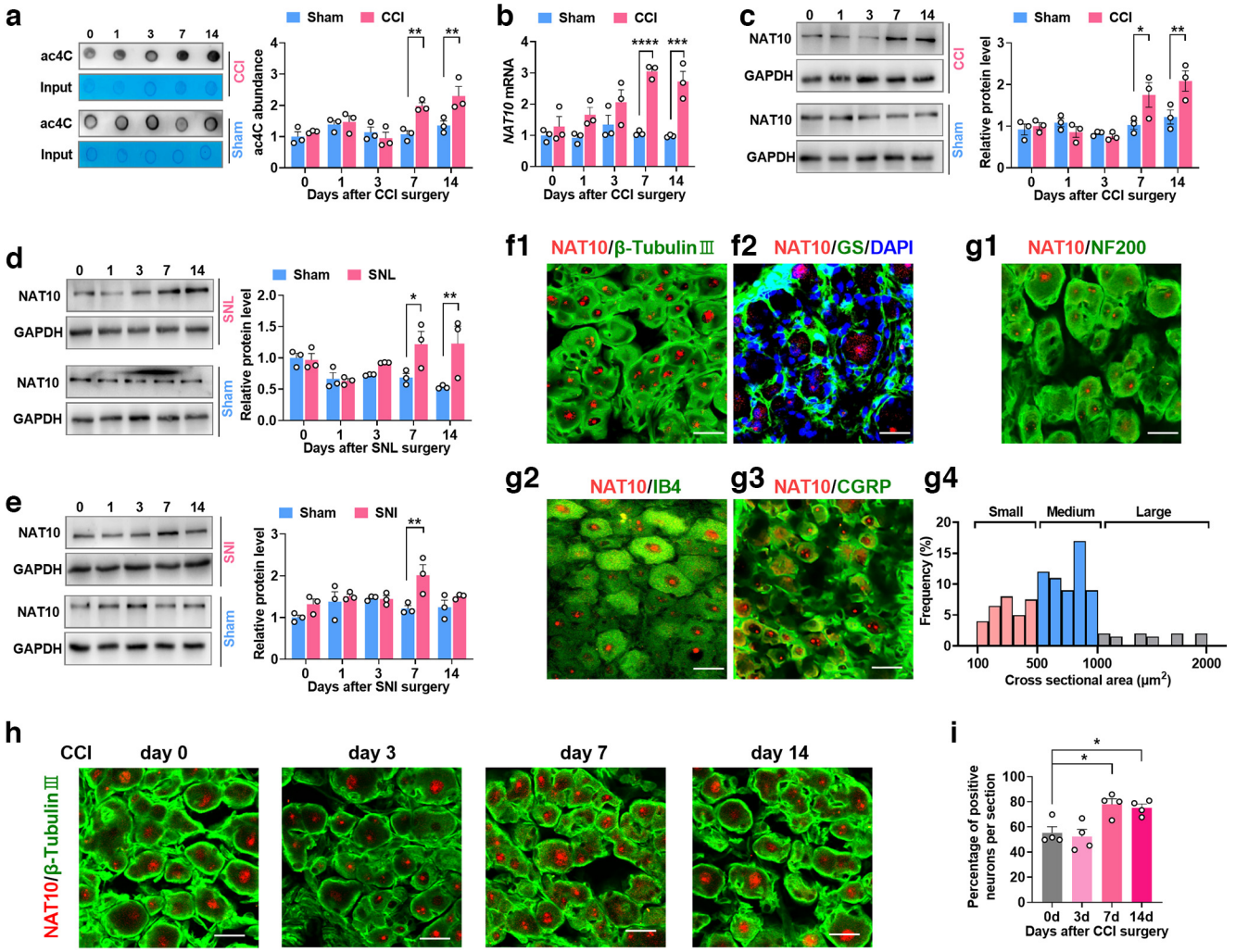

Figure 1. Neuropathic pain increases the levels of overall ac4C and NAT10 protein in injured DRG. ***a***, Time course of changes in ipsilateral ac4C in L3/4 DRGs after chronic constriction injury (CCI) or sham surgery of the unilateral sciatic nerve. $n = 6$ mice/time point/group, $^{**}p < 0.01$ versus the corresponding sham group; two-way ANOVA, *post hoc* Tukey's test. Total of 4 DRGs from two mice were pooled to be one sample. The collected L3/4 DRGs were subjected to RNA extraction, dot-blotted and incubated with an ac4C-specific antibody. ***b***, Quantitative analysis of *Nat10* mRNA expression in ipsilateral L3/4 DRGs by qRT-PCR at 0, 1, 3, 7, and 14 d after CCI or sham surgery. $n = 6$ mice/group, $^{***}p < 0.001$, $^{****}p < 0.0001$ versus the sham group; two-way ANOVA, *post hoc* Tukey's test. ***c–e***, Expression of NAT10 protein in ipsilateral and contralateral L3/4 DRGs at different times after CCI (***c***), spinal nerve ligation (SNL; ***d***), and spared nerve injury (SNI; ***e***). $n = 6$ mice/group, $^{*}p < 0.05$, $^{**}p < 0.01$ versus the sham group; two-way ANOVA, *post hoc* Tukey's test. ***f1***, ***f2***, NAT10 (red) is co-expressed with β-Tubulin III (green, a neuronal marker; ***f1***) or glutamine synthetase (GS; green, a microsatellite glia cell marker; ***f2***)-labeled DRG cells; $n = 4$ repeats. Scale bar, 30 μm. ***g1–g4***, NAT10 (red)-positive neurons co-labeled with neurofilament-200 (NF200, green; ***g1***), isolectin B4 (IB4, green; ***g2***), and calcitonin gene-related peptide (CGRP; green; ***g3***), and the distribution of NAT10-positive somata in the normal mouse L3/4 DRGs: small 27%, medium 52%, and large 21% (***g4***). $n = 6$ repeats. Scale bar, 30 μm. ***h, i,*** Number of the neurons labeled by NAT10 (red) in the ipsilateral L3/4 DRGs on days 0, 3, 7, and 14 after CCI surgery (***h***). $n = 8$ mice/group, $^{*}p < 0.05$ versus CCI day 0 group; one-way ANOVA, *post hoc* Tukey's test (***i***). Scale bar, 30 μm. See Extended Data Figure 1-1.

Fig. 1-1*c*). To summarize, we found that peripheral nerve injury upregulates the levels of ac4C and NAT10 in the ipsilateral DRG.

Next, we examined the distribution of NAT10 in DRG cells. Double-staining assays showed that NAT10 staining overlaps with β-Tubulin III (a neuronal marker), but not with glutamine synthetase (GS; a marker of adjacent satellite glial cells), indicating that NAT10 is predominantly expressed in DRG neurons (Fig. 1*f*). In addition, 28.7% of NAT10-positive neurons were calcitonin gene-related peptide (CGRP)-labeled cells (small peptidergic DRG neurons), and 50.3% were isolectin B4 (IB4)-labeled cells (small nonpeptidergic neurons). Only 21% of NAT10-labeled neurons were positive for neurofilament-200 (NF200; a marker of medium/large cells and myelinated Aβ-fibers; Fig. 1*g1–g3*; Extended Data Fig. 1-1*d*). Consistent with this, an analysis of the cross-sectional area of neuronal somata revealed that ~27% of NAT10-positive neurons were small (area <600 μm^2), 52% were medium-sized (area = 600–1000 μm^2), and 21% were large (area >1000 μm^2; Fig. 1*g4*). These distribution patterns support the hypothesis that NAT10 participates in the transmission/modulation of nociceptive information. As expected, the number of NAT10-positive neurons in the ipsilateral L3/4 DRGs was increased by 42% on day 7 and 36.1% on day 14 after CCI injury, compared with day 0 (Fig. 1*h,i*). Collectively, those results suggest that neuropathic pain leads to increases in both ac4C and NAT10 in peripheral sensory neurons.

A CCI-induced increase in DRG USF1 is responsible for NAT10 upregulation

How is NAT10 upregulated in the DRG after CCI-induced neuropathic pain? Transcription factors can control gene expression by binding to the gene promoter, so we focused on the transcription-factor mechanism underlying NAT10 expression. First, we performed an informatics analysis of the transcription factors binding to the Nat10 promoter using the online JASPAR program and

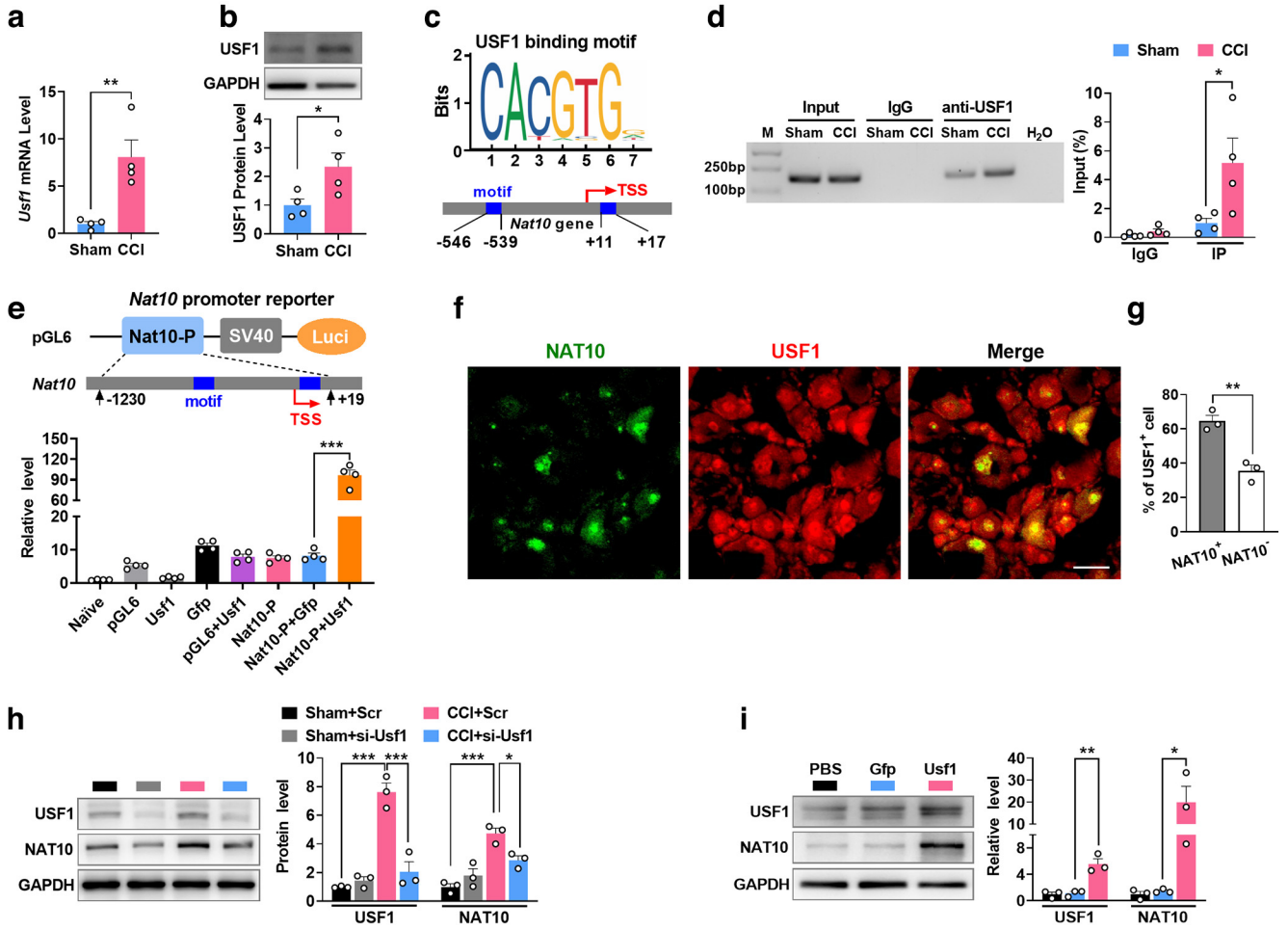

Figure 2. USF1 upregulation activates NAT10 expression in injured DRG following peripheral nerve injury. ***a***, ***b***, The level of *Usf1* mRNA (***a***) and USF1 protein (***b***) expression in ipsilateral L3/4 DRGs on day 7 after CCI. $n = 8$ mice/group, $^{*}p < 0.05$, $^{**}p < 0.01$ versus the sham group; two-tailed unpaired Student's test. ***c***, Two *Usf1* binding motif regions located, respectively, in −546 to −539 and +11 to +17 of mouse *Nat10* promoter (transcription start site designated as +1). ***d***, *Nat10* promoter fragment immunoprecipitated by rabbit anti-USF1 antibody in the ipsilateral L3/4 DRGs on day 7 after CCI or sham surgery. Input: total purified fragments. IgG: purified rabbit IgG. M: DNA ladder marker. $n = 16$ mice/group. $^{*}p < 0.05$ versus the sham group; two-tailed unpaired Student's *t* test. ***e***, *Nat10* promoter activity in HEK-293T cells transfected as shown. Naive: no treatment. pGL6: empty vector control. Usf1: lentivirus expressing full-length *Usf1*. Gfp: lentivirus expressing *Gfp* control. Nat10-P: pGL6 reporter with *Nat10* promoter. $n = 4$ repeats. $^{***}p < 0.001$ versus the Nat10-P-plus-Gfp; one-way ANOVA test, *post hoc* Tukey's test. ***f***, ***g***, Double-immunofluorescence staining of USF1 with NAT10 (***f***), and analysis of their co-expression (***g***) in DRG; $n = 3$ repeats. Scale bar, 30 μm. $^{**}p < 0.01$, two-tailed unpaired Student's *t* test. ***h***, Level of USF1 and NAT10 protein in the ipsilateral L3/4 DRGs 7 d after CCI surgery with microinjection of *Usf1*-siRNA after surgery. $n = 6$ mice/group, $^{*}p < 0.05$, $^{***}p < 0.001$ versus corresponding groups; one-way ANOVA, *post hoc* Tukey's test. ***i***, Level of USF1 and NAT10 protein in L3/4 DRGs with microinjection of Lenti-*Usf1* (Usf1) or Lenti-*Gfp* (Gfp) on day 5 after injection. $n = 6$ mice/group, $^{*}p < 0.05$, $^{**}p < 0.01$ versus Lenti-*Gfp* group; one-way ANOVA test, *post hoc* Tukey's test. See Extended Data Figure 2-1.

identified a consensus binding motif (5′-CACGTG-3′) for upstream transcription factor 1 (USF1) in the promoter region of Nat10. Usf1 mRNA and protein were both increased in the DRG of CCI mice (Fig. 2*a*,*b*), consistent with increases in NAT10. There are two consensus USF1 binding motif (5′-CACGTG-3′; Zeng et al., 2018) regions (−546 to −539 and +11 to +17, transcription start site designated as +1) in the Nat10 promotor (Fig. 2*c*). A chromatin immunoprecipitation (ChIP) assay showed that the binding motif could be amplified from the complex immunoprecipitated with a USF1 antibody in nuclear fractions from the DRGs of both sham and CCI mice, but the binding fragment number was increased 5-fold in the ipsilateral L3/4 DRGs on day 7 post-CCI surgery, compared with sham mice (Fig. 2*d*). This increase was due at least partly to a marked upregulation of USF1 in the DRG after CCI nerve injury (Fig. 2*b*). Next, a 1249-bp-length Nat10 promoter fragment containing the two binding motifs was inserted upstream of pGL6, a luciferase report vector, and co-transfected into HEK293T cells with the full-length USF1 expression plasmid. As expected, the pGL6 reporter exhibited an increase in luciferase activity compared with the empty pGL6 vector. Co-transfection of the USF1 expression plasmid, but not the control GFP plasmid, further increased the luciferase activity of the pGL6 reporter 96-fold (Fig. 2*e*). This *in vitro* assay indicates that USF1 promotes the expression of NAT10.

Next, we examined the expression pattern of USF1 in the DRG. Double-labeling showed that USF1 was predominantly co-expressed with β-Tubulin III, but not with GS, indicating that USF1 is mainly located in DRG neurons (Extended Data Fig. 2-1*c*,*d*). Moreover, 64% USF1-positve cells expressed NAT10 (Fig. 2*f*,*g*). To address whether USF1 participates in neuropathic pain, we used siRNA to knock down USF1 in CCI mice and packaged lentivirus to express full-length USF1 in naive mice. Microinjection of *Usf1* siRNA, but not its control scrambled siRNA, into L3/4 DRGs reduced both USF1 and NAT10 expression on day 4 after injection in CCI mice (Fig. 2*h*). Behaviorally, consistent with previous studies (Pan et al., 2021b), nerve injury caused increased ipsilateral paw-withdrawal frequencies in response to mechanical stimuli [low (0.07 g) and medium (0.4 g) force von Frey filaments;

Extended Data Fig. 2-1*e*,*f*] and the decreased paw-withdrawal latencies in response to heat stimuli (Extended Data Fig. 2-1*g*), indicating mechanical allodynia and heat hyperalgesia. USF1 knock-down with siRNA alleviated the hypersensitivity to mechanical and thermal stimuli from days 3 to 6 after injection in CCI mice; USF1 knock-down did not affect normal responses to mechanical and heat stimuli in sham animals (Extended Data Fig. 2-1*e*–*g*). Microinjection of Usf1 siRNA did not impair locomotor behavior in either sham or CCI mice (Table 2). Microinjection of Lenti-Usf1 into L3/4 DRGs of naive mice not only increased expression of USF1 and NAT10 on day 5 after injection (Fig. 2*i*), but also induced neuropathic pain-like behavior, demonstrated by enhanced hypersensitivity to mechanical and thermal stimulus from day 4 after lentivirus injection (Extended Data Fig. 2-1*h*–*j*). Lentivirus injection did not alter locomotor function (Table 2). Our data strongly support the hypothesis that nerve-injury-induced NAT10 upregulation can be attributed, at least in part, to increased USF1 expression in injured DRGs.

Table 2. Test of locomotor function after injection of manipulation tools

	Locomotor function test		
Treatment groups	Placing	Grasping	Righting
PBS (1 μl)	5(0)	5(0)	5(0)
Sham + Scr	5(0)	5(0)	5(0)
Sham+si-*Nat10*	5(0)	5(0)	5(0)
Sham+si-*Syt9*	5(0)	5(0)	5(0)
Sham+si-*Usf1*	5(0)	5(0)	5(0)
CCI + Scr	5(0)	5(0)	5(0)
CCI+si-*Nat10*	5(0)	5(0)	5(0)
CCI+si-*Syt9*	5(0)	5(0)	5(0)
CCI+si-*Usf1*	5(0)	5(0)	5(0)
Lenti-*Nat10*	5(0)	5(0)	5(0)
Lenti-*Syt9*	5(0)	5(0)	5(0)
Lenti-*Usf1*	5(0)	5(0)	5(0)
Lenti-*GFP*	5(0)	5(0)	5(0)
Sham+Scr	5(0)	5(0)	5(0)
Sham+shRNA	5(0)	5(0)	5(0)
CCI+Scr	5(0)	5(0)	5(0)
CCI+shRNA	5(0)	5(0)	5(0)
AAV-GFP+Sham	5(0)	5(0)	5(0)
AAV-GFP+CCI	5(0)	5(0)	5(0)
AAV-Cre+Sham	5(0)	5(0)	5(0)
AAV-Cre+CCI	5(0)	5(0)	5(0)
Lenti-GFP+Scr	5(0)	5(0)	5(0)
Lenti-GFP+si-*Syt9*	5(0)	5(0)	5(0)
Lenti-GFP+si-*Nat10*	5(0)	5(0)	5(0)
Lenti-*Nat10*+Scr	5(0)	5(0)	5(0)
Lenti-*Nat10*+si-*Syt9*	5(0)	5(0)	5(0)
Lenti-*Usf1*+Scr	5(0)	5(0)	5(0)
Lenti-*Usf1*+si-*Nat10*	5(0)	5(0)	5(0)
gRNA-Scr+dCasRx-*Nat10*	5(0)	5(0)	5(0)
gRNA-27+ dCasRx-*Nat10*	5(0)	5(0)	5(0)
gRNA-153+ dCasRx-*Nat10*	5(0)	5(0)	5(0)

Data are mean (SEM). $n = 8$/group; no significance; one-way ANOVA (response time vs treated groups) followed by *post hoc* Tukey's test.

Downregulation of DRG NAT10 attenuates CCI-induced nociceptive responses

Next, we asked whether NAT10 is involved in neuropathic pain. First, we designed two siRNAs for use in the following experiment. Nat10-siRNA-566 (translation start site designated as +1) decreased the expression of Nat10 mRNA *in vitro* by 45.2% but Nat10-siRNA-1138 had no effect on Nat10 expression (Extended Data Fig. 3-1*a*). Therefore, we used Nat10-siRNA-566 in the *in vivo* experiment. Microinjection of Nat10-siRNA-566 after CCI blocked the nerve-injury-induced increase in NAT10 in the ipsilateral DRG (Fig. 3*a*). Furthermore, we observed that downregulation of NAT10 via DRG microinjection of Nat10-siRNA ameliorated the CCI-induced heat and mechanical hypersensitivity (Fig. 3*b*–*d*). Microinjection of scrambled siRNA did not have a similar analgesic effect during the observation period (Fig. 3*b*–*d*) and Nat10-siRNA treatment changed neither the contralateral thresholds in CCI mice nor the ipsilateral responses in sham mice (Fig. 3*b*–*d*; Extended Data Fig. 3-1*b*–*d*). As expected, Nat10-siRNA microinjection, but not the scrambled control, impaired CCI-induced hyperactivity in neurons of the spinal dorsal horn: Nat10-siRNA microinjection abolished CCI-induced increases in the phosphorylation of extracellular-signal-regulated kinase 1 and 2 (p-ERK1/2; a marker of neuronal hyperactivation) and glial fibrillary acidic protein (GFAP; a marker of astrocytic hyperactivation) in the ipsilateral L3/4 dorsal horn (Fig. 3*e*). Next, we converted the Nat10-siRNA-566 sequence to lentivirus shRNA and microinjected this into L3/4 DRGs 2 d before surgery (preinjection) or 7 d after surgery (postinjection) to endogenously express shRNA in CCI or sham mice. Preinjection or postinjection of Nat10-shRNA (but not control Scr-shRNA) not only inhibited the CCI-induced increase in NAT10 in ipsilateral L3/4 DRGs (Fig. 3*f*), but also alleviated CCI-induced pain hypersensitivity in the ipsilateral paws (Fig. 3*g*–*l*), while having no influence on the contralateral side (Extended Data Fig. 3-1*f*–*h*). No locomotor impairments were seen in either sham or CCI mice after injection of Nat10-siRNA or -shRNA or their controls (Table 2). As expected, shRNA-induced NAT10 knock-down reversed the increases in p-ERK1/2 and GFAP levels in the ipsilateral L3/4 dorsal horn of CCI mice, compared with the scrambled control (Fig. 3*m*).

Given that siRNA and shRNA may have potential off-target effects, we generated $Nat10^{fl/fl}$ mice (Extended Data Fig. 3-1*i*), in which DRG NAT10 is specifically knocked out in the presence of Cre recombinase. By microinjecting AAV-Cre into the DRG, we could thus measure the effect of genetic deletion of DRG NAT10 on pain behavior. As expected, preinjection of AAV-Cre into the DRG of $Nat10^{fl/fl}$ mice three weeks before CCI/sham surgery blocked the CCI-induced elevation of NAT10 on day 7 after surgery, compared with the AAV-Gfp group (Fig. 3*n*). $Nat10^{fl/fl}$ mice preinjected with AAV-Cre, but not AAV-Gfp, showed slight pain hypersensitivity to mechanical and thermal stimuli on day 7 after CCI surgery (Fig. 3*o*–*q*). AAV-Cre and the control Gfp treatments did not affect the locomotor responses of $Nat10^{fl/fl}$ mice after CCI surgery (Table 2). NAT10 knock-out with AAV-Cre, but not AAV-Gfp, diminished CCI-induced upregulation of p-ERK1/2 and GFAP in $Nat10^{fl/fl}$ mice (Fig. 3*r*). Thus, our data suggest that DRG NAT10 plays an essential role in the initiation and maintenance of neuropathic pain.

Mimicking the NAT10 increase produces neuropathic-pain-like behavior

We set out to examine whether upregulation of DRG NAT10 is sufficient for the induction of nociceptive hypersensitivity. We constructed a full-length Nat10 lentivirus expression vector. Compared with the control Lenti-Gfp, microinjection of Lenti-Nat10 in L3/4 DRGs enhanced the expression of NAT10 by 213% on day 6 after injection (Fig. 4*a*). Lenti-Nat10-mediated upregulation also led to a dramatic increase in the ipsilateral paw-withdrawal frequencies to the 0.07- and 0.4-g stimuli (Fig. 4*b*,*c*)

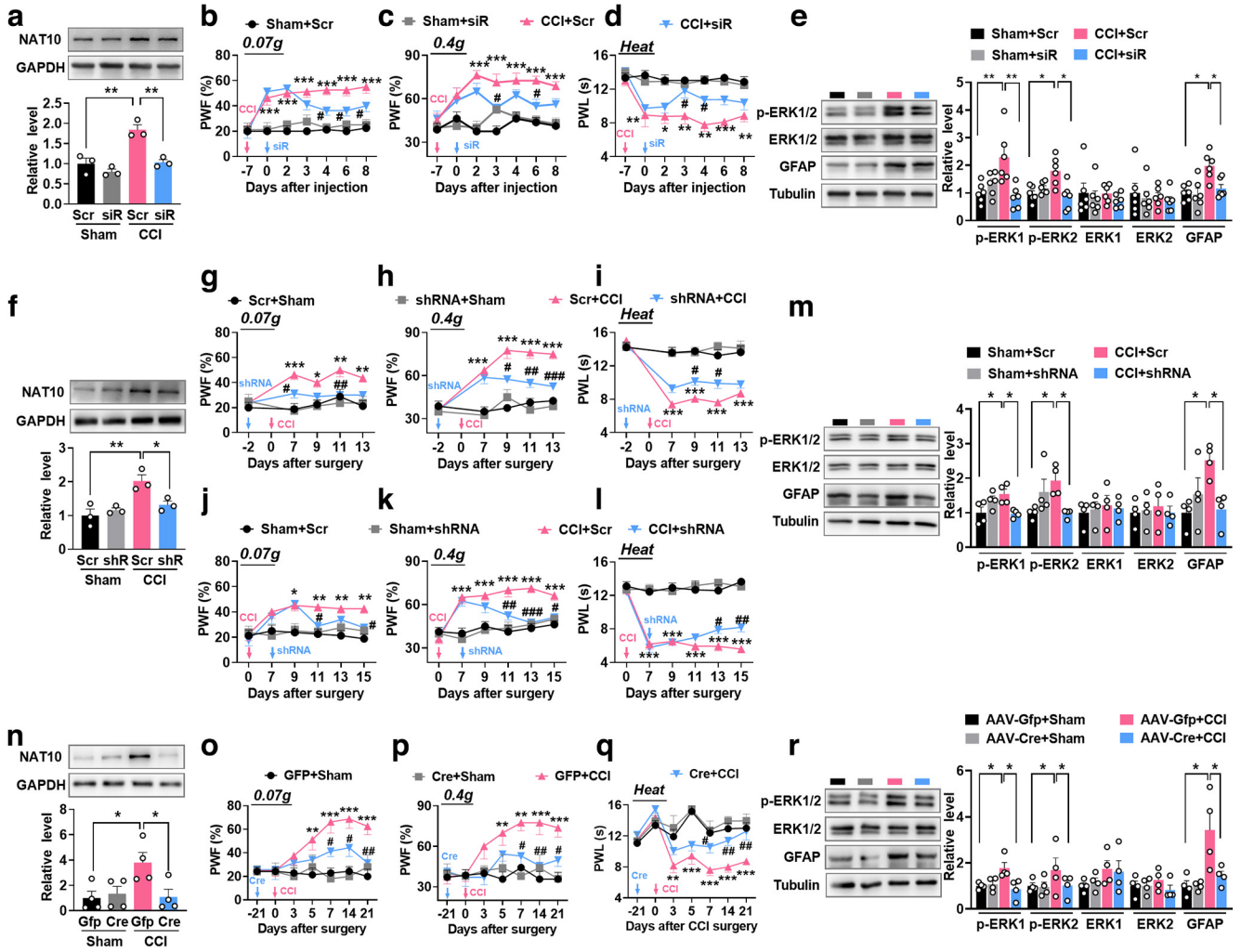

Figure 3. Increased DRG NAT10 is required for induction and maintenance of neuropathic pain. ***a***, NAT10 protein expression 3 d after DRG microinjection of *Nat10*-siRNA (siR) or scrambled siRNA (Scr) into the L3/4 DRGs of mice, 7 d post-CCI. $n = 6$ mice/group, $^{**}p < 0.01$ versus the corresponding groups; one-way ANOVA, *post hoc* Tukey's test. ***b–d***, Time course of the effect of microinjection of *Nat10*-siRNA (siR) or scrambled siRNA (Scr) into unilateral L3/4 DRGs of CCI or sham mice on the paw-withdrawal frequency (PWF) to 0.07 g (***b***) and 0.4 g (***c***) von Frey filaments and on paw-withdrawal latencies (PWL) to heat stimuli (***d***) on the ipsilateral side. $n = 8$ mice/group, $^{*}p < 0.05$, $^{**}p < 0.01$, $^{***}p < 0.001$ versus the sham-plus-Scr group at the corresponding time points. $\#p < 0.05$ versus the CCI-plus-Scr group at the corresponding time points; two-way ANOVA, *post hoc* Tukey's tests. Red arrow, CCI or sham surgery. Blue arrows, *Nat10*-siRNA or Scr injection. ***e***, Level of phosphorylation of extracellular signal-regulated kinase 1 and 2 (p-ERK1/2, a marker of neuronal hyperactivation) in the ipsilateral dorsal spinal horn on day 3 after microinjection of *Nat10*-siRNA or scrambled siRNA into the L3/4 DRGs of mice 7 d post-CCI or sham surgery. $n = 6$ mice/group, $^{*}p < 0.05$, $^{**}p < 0.01$ versus the corresponding groups; two-way ANOVA, *post hoc* Tukey's test. ***f***, DRG NAT10 expression on day 5 after microinjection of Lenti-*Nat10*-shRNA (shR) or its scrambled shRNA (Scr) into the L3/4 DRGs in mice 7 d post-CCI or sham surgery. $n = 6$ mice/group, $^{*}p < 0.05$, $^{**}p < 0.01$ versus the corresponding groups; one-way ANOVA test, *post hoc* Tukey's test. ***g–i***, Effect of preinjection of Lenti-*Nat10*-shRNA (shRNA) or its scrambled shRNA (Scr) into the unilateral L3/4 DRGs 2 d before CCI or sham surgery on mechanical allodynia (***g***, ***h***) and thermal hyperalgesia (***i***) on the ipsilateral side. $n = 8$ mice/group, $^{*}p < 0.05$, $^{**}p < 0.01$, $^{***}p < 0.001$ versus the Scr-plus-sham group at the corresponding time points; $\#p < 0.05$, $\#\#p < 0.01$, $\#\#\#p < 0.001$ versus the Scr-plus-CCI group at the corresponding time points; two-way ANOVA, *post hoc* Tukey's test. Red arrow, CCI or sham surgery. Blue arrows, *Nat10*-shRNA or Scr. ***j–l***, Effect of postinjection of Lenti-*Nat10*-shRNA or its control into the unilateral L3/4 DRGs on day 7 after CCI or sham surgery on ipsilateral mechanical allodynia (***j***, ***k***) and thermal hyperalgesia (***l***). $n = 8$ mice/group, $^{*}p < 0.05$, $^{**}p < 0.01$, $^{***}p < 0.001$ versus the sham-plus-Scr group at the corresponding time points; $\#p < 0.05$, $\#\#p < 0.01$, $\#\#\#p < 0.001$ versus the CCI-plus-Scr group at the corresponding time points; two-way ANOVA, *post hoc* Tukey's test. Red arrow, CCI or sham surgery. ***m***, The level of p-ERK1/2 in the ipsilateral dorsal horn on day 5 after postinjection of *Nat10*-shRNA or the scrambled control into L3/4 DRGs in CCI or sham mice. $n = 4$ mice/group, $^{*}p < 0.05$ versus the corresponding groups; two-way ANOVA, *post hoc* Tukey's test. ***n***, Ipsilateral DRG NAT10 level on day 21 after preinjection of rAAV-hSyn-*Cre* (Cre) or rAAV-hSyn-*Gfp* (Gfp) into L3/4 DRGs of Nat10$^{f/f}$ mice before CCI or sham surgery. $n = 8$ mice/group, $^{*}p < 0.05$ versus the corresponding groups; one-way ANOVA, *post hoc* Tukey's test. ***o–q***, Mechanical (***o***, ***p***) and thermal (***q***) pain thresholds from day 21 after preinjection of rAAV-hSyn-*Cre* or rAAV-hSyn-*Gfp* into L3/4 DRGs of Nat10$^{f/f}$ mice before CCI or sham surgery. $n = 8$ mice/group, $^{**}p < 0.01$, $^{***}p < 0.001$ versus the Gfp-plus-sham groups; $\#p < 0.05$, $\#\#p < 0.01$ versus the Gfp-plus-CCI group at the corresponding time points; two-way ANOVA, *post hoc* Tukey's test. ***r***, The level of p-ERK1/2 expression in the ipsilateral dorsal horn on day 7 after CCI in Nat10$^{f/f}$ mice preinjected with rAAV-hSyn-*Cre* or rAAV-hSyn-*Gfp* into L3/4 DRGs. $n = 4$ mice/group, $^{*}p < 0.05$ versus the corresponding groups; two-way ANOVA, *post hoc* Tukey's test. See Extended Data Figure 3-1.

and a marked decrease in the ipsilateral paw-withdrawal latency to heat (Fig. 4*d*) from day 4 after microinjection to the end of the observation period. However, the Lenti-Nat10-mediated upregulation did not change the mechanical and heat responses on the contralateral side (Fig. 4*e–g*), and microinjection of Lenti-Gfp had no effect on behavioral responses. Robust increases in the levels of p-ERK1/2 and GFAP were detected in the ipsilateral dorsal horn of the spinal cord on day 6 after Lenti-Nat10 microinjection, indicating hyperactivity of neurons and astrocytes (Fig. 4*h*). No locomotor changes were observed in either the Lenti-Nat10 or Lenti-Gfp mice (Table 2).

Finally, we explored whether NAT10 mediates the USF1-induced pain responses. We found that DRG microinjection of Nat10-siRNA not only reversed the upregulation of NAT10

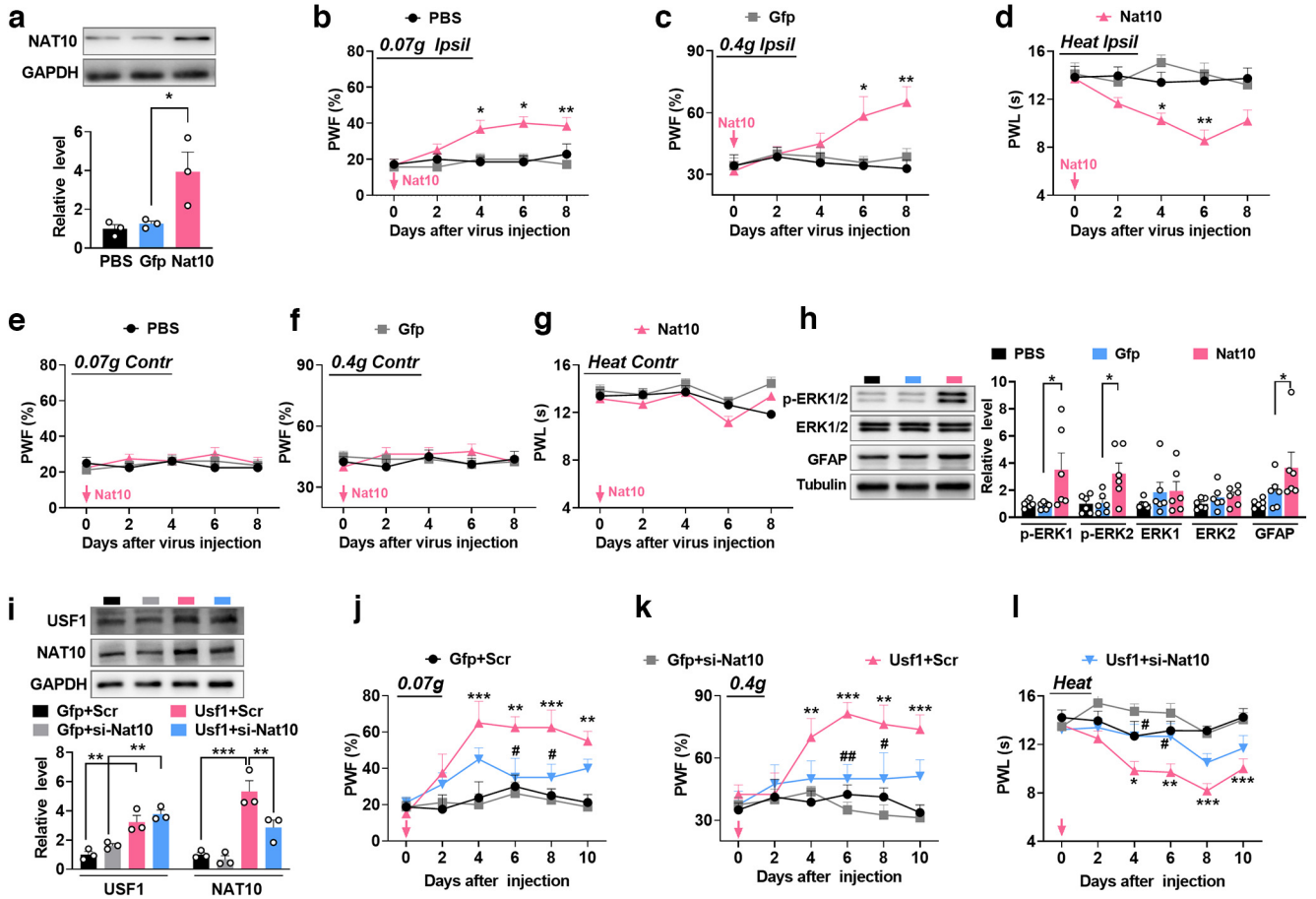

Figure 4. Upregulating DRG NAT10 expression induces neuropathic pain. ***a***, NAT10 levels in the ipsilateral L3/4 DRGs on day 6 after microinjection of Lenti-*Nat10* (Nat10) or control Lenti-*Gfp* (Gfp) into unilateral L3/4 DRGs in naive mice. $n = 6$ mice/group. $^{*}p < 0.05$, versus Gfp group; one-way ANOVA, *post hoc* Tukey's test. ***b–d***, Time line of the effect of microinjection of Lenti-*Nat10* (Nat10) or control Lenti-*Gfp* (Gfp) into unilateral L3/4 DRGs on the paw-withdrawal frequency (PWF) to 0.07 g (***b***) and 0.4 g (***c***) von Frey filaments and on paw-withdrawal latencies (PWLs) to heat stimuli (d) on the ipsilateral side at the different days after lentivirus microinjection. $n = 8$ mice/group. $^{*}p < 0.05$, $^{**}p < 0.01$ versus Gfp-treated mice at the corresponding time points; two-way ANOVA, *post hoc* Tukey's test. ***e–g***, As for ***b–d*** but for the contralateral side. $n = 8$ mice/group. ***h***, Detection of p-ERK1/2 and GFAP levels in the ipsilateral L3/4 dorsal spinal horn on day 7 after microinjection with Lenti-*Nat10* (Nat10) or control Lenti-*Gfp* (Gfp) into unilateral L3/4 DRGs. $n = 6$ mice/group. $^{*}p < 0.05$ versus Gfp group; two-way ANOVA, *post hoc* Tukey's test. ***i***, USF1 and NAT10 protein levels in the ipsilateral L3/4 DRGs after microinjection of Lenti-*Usf1* (Usf1) and *Nat10*-siRNA (si-Nat10). Gfp, Lenti-*Gfp*. Scr, scrambled siRNA. $n = 6$ mice/group. $^{**}p < 0.01$, $^{***}p < 0.001$ versus the corresponding groups; two-way ANOVA, *post hoc* Tukey's test. ***j–l***, Microinjection of si-*Nat10* alleviates the mechanical allodynia (***j***, ***k***) and heat hyperalgesia (***l***) caused by USF1 upregulation. $n = 8$ mice/group, $^{*}p < 0.05$, $^{**}p < 0.01$, $^{***}p < 0.001$ versus the Lenti-*Gfp*-plus-Scr group at the corresponding time points. $\#p < 0.05$, $\#\#p < 0.01$ versus the Lenti-*Usf1*-plus-Scr group at the corresponding time points; two-way ANOVA, *post hoc* Tukey's test.

protein induced by microinjection of Lenti-Usf1 (Fig. 4*i*), but also alleviated the heat and mechanical hyperalgesia induced by upregulation of USF1 (Fig. 4*j–l*). These observations suggest that, in the absence of nerve injury, DRG NAT10 upregulation likely leads to neuropathic pain-like symptoms.

NAT10 contributes to enhanced efficiency of global protein synthesis in nerve-injured DRG

N4-acetylation of cytidine (ac4C) in mRNA by the acetyltransferase NAT10 promotes protein translation efficiency (Arango et al., 2018). To investigate whether ac4C is involved in the regulation of protein translation in the DRG under conditions of neuropathic pain, we employed dot-blot (Arango et al., 2018) and SUnSET (surface sensing of translation; Schmidt et al., 2009) assays to evaluate alterations in global ac4C and nascent proteins level after manipulating NAT10 expression. A dot-blot assay with an ac4C antibody showed that the CCI-induced ac4C increase in L3/4 DRGs was hindered by NAT10 knockdown by siRNA on day 3 after microinjection (Fig. 5*a*) or by shRNA on day 4 after microinjection (Fig. 5*b*) in CCI mice. Preinjection of AAV2-Syn-Cre on day 21 before surgery abolished the increase in ac4C level in L3/4 DRGs in CCI $Nat10^{fl/fl}$ mice (Fig. 5*c*). Furthermore, in the SUnSET assay, in which nascent proteins are labeled with puromycin via intraperitoneal injection 1 h before harvesting the DRG, nerve injury caused an increase in nascent proteins in L3/4 DRGs; this increase was significantly reduced in CCI mice by microinjection of Nat10-siRNA but not the scrambled control (Fig. 5*e*,*f*). NAT10 overexpression through microinjection of Lenti-Nat10, but not Lenti-Gfp, evoked an increase in global ac4C (Fig. 5*d*) and resulted in the elevation of nascent proteins in L3/4 DRGs on day 4 after injection (Fig. 5*g*,*h*). Collectively, these data suggest that CCI leads to increased efficiency of de novo protein synthesis as a result of enhanced levels of ac4C, which in turn are because of increased expression of NAT10.

NAT10 positively regulates SYT9 expression in injured DRG after CCI

To explore the downstream mechanisms underlying the involvement of NAT10 in nociceptive behavior, we used tandem mass tags (TMT; Friedrich et al., 2021) to identify targets regulated by

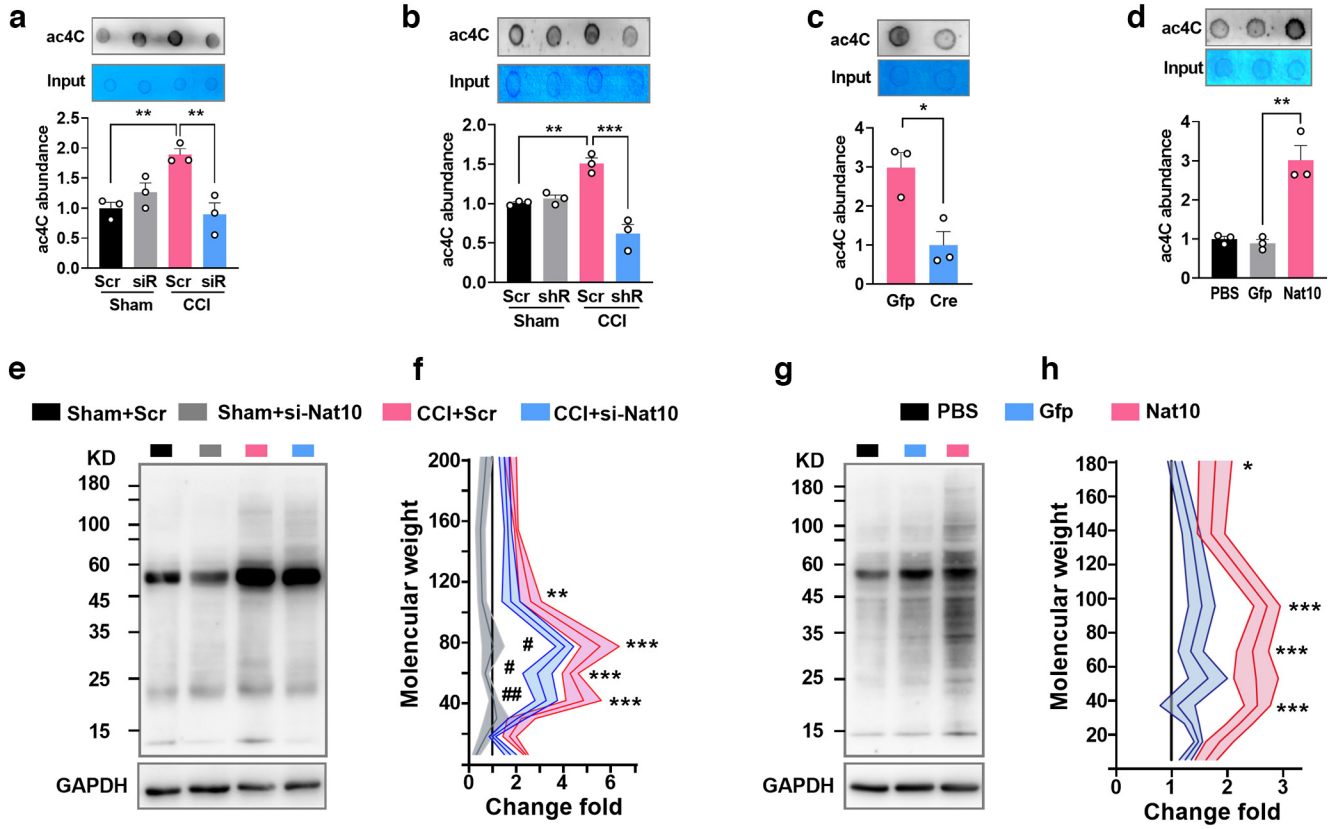

Figure 5. NAT10 promotes enhanced protein synthesis efficiency in the DRG after nerve injury. ***a***, The level of ac4C in ipsilateral L3/4 DRGs on day 3 after microinjection of *Nat10*-siRNA (siRNA) or scrambled siRNA (Scr) into unilateral L3/4 DRGs of CCI mice. $n = 6$ mice/group, $^{**}p < 0.01$ versus the corresponding groups; one-way ANOVA, *post hoc* Tukey's test. ***b***, The overall ac4C level in ipsilateral L3/4 DRGs on day 5 after microinjection of Lenti-*Nat10*-shRNA (shR) or scrambled shRNA (Scr) into unilateral L3/4 DRGs of CCI mice. $n = 6$ mice/group, $^{**}p < 0.01$, $^{***}p < 0.001$ versus the corresponding groups; one-way ANOVA, *post hoc* Tukey's test. ***c***, The overall ac4C level in ipsilateral L3/4 DRGs on day 7 after CCI or sham surgery in *Nat10*$^{fl/fl}$ mice pre-injected with AAV2-Syn-*Cre* (Cre) or AAV2-Syn-*Gfp* (Gfp) into unilateral L3/4 DRGs 21 d before surgery. $n = 6$ mice/group, $^{*}p < 0.05$ versus Gfp group; two-tailed unpaired Student's *t* test. ***d***, The level of overall ac4C in ipsilateral L3/4 DRGs on day 6 after microinjection of Lenti-*Nat10* (Nat10) or Lenti-*Gfp* (Gfp) into unilateral L3/4 DRGs in naive mice. $n = 6$ mice/group. $^{**}p < 0.01$ versus Gfp control; one-way ANOVA, *post hoc* Tukey's test. ***e***, ***f***, SUnSET assay detection for global nascent protein levels in L3/4 DRGs on day 3 after microinjection of *Nat10*-siRNA (si-Nat10) or scrambled siRNA (Scr) into unilateral L3/4 DRGs of CCI mice. $n = 9$ mice/group, $^{**}p < 0.01$, $^{***}p < 0.001$ versus the sham-plus-Scr groups; $\#p < 0.05$, $\#\#p < 0.01$ versus CCI-plus-Scr groups; two-way ANOVA, *post hoc* Tukey's test. DRGs were collected 1 h after intraperitoneal injection of puromycin and used for Western blotting to analyze global protein levels. ***g***, ***h***, The level of global nascent proteins in L3/4 DRGs on day 6 after microinjection of Lenti-*Nat10* (Nat10) or Lenti-*Gfp* (Gfp) into unilateral L3/4 DRGs in naive mice. $n = 9$ mice/group, $^{*}p < 0.05$, $^{***}p < 0.001$ versus Gfp group; two-way ANOVA, *post hoc* Tukey's test.

NAT10 in injured DRG. In the unbiased protein profiles, 6580 proteins were identified in total. CCI mice in the ipsilateral L3/4 DRGs on postsurgery day 7 showed significant changes in 952 of these 3 d after the microinjection, relative to sham mice. Of the altered proteins, 79.62% were upregulated and 20.38% were downregulated (Fig. 6*a*). Microinjection of Nat10-siRNA on day 7 post-CCI reversed 74 of the CCI-induced upregulated proteins (Fig. 6*b*). These affected proteins are notably enriched for proteins involved in the calcium-dependent activation of synaptic vesicle fusion (Fig. 6*c*).

Notably, in the protein mass spectrometry results, the CCI-induced increase in SYT9 was significantly reversed by NAT10 downregulation in the L3/4 DRGs (Fig. 6*b*, outlined in blue). SYT9 belongs to the synaptotagmin family, which regulates exocytosis by fine-tuning Ca^{2+}-dependent neurotransmitter release from synaptic vesicles (Wolfes and Dean, 2020). Thus, we selected SYT9 as a potential target. Western blot assays confirmed that DRG microinjection of Nat10-siRNA inhibited the CCI-induced elevation in the level of SYT9 protein in the ipsilateral L3/4 DRGs on day 7 after CCI (Fig. 6*d*). Interestingly, qRT-PCR results show that CCI did not change the expression of Syt9 mRNA, and expression was not affected by NAT10 knock-down with siRNA treatment (Fig. 6*e*). By contrast, upregulation of NAT10 by microinjection of Lenti-Nat10 (but not the Lenti-Gfp control) dramatically increased the amount of SYT9 protein in the injected DRG on day 5 after microinjection in naive mice (Fig. 6*f*), but did not alter the level of Syt9 mRNA (Fig. 6*g*), indicating that NAT10 may regulate SYT9 via a posttranscriptional mechanism. To verify this, we used polysome fractionation assays (Panda et al., 2017) to evaluate the effect of NAT10 on the translation efficiency of Syt9 mRNA. qRT-PCR results show that nerve injury enhanced ribosomal binding to Syt9 mRNA in L3/4 DRGs (mainly in the polysomal fraction) and that Nat10-siRNA knock-down blocked this increase, with Syt9 mRNA detected mainly in the monosomes or light polysomes in this condition (Fig. 6*h*).

Overexpressing NAT10 with Lenti-Nat10 dramatically increased the amount of Syt9 mRNA in the polysomal fractions on day 5 after microinjection in naive mice, compared with the Lenti-Gfp group (Fig. 6*i*). These data indicate that the enhanced translation efficiency of Syt9 with nociception likely resulted from NAT10 upregulation. Moreover, double immunofluorescent labeling revealed that almost 70% of SYT9-positive cells co-expressed NAT10 (Fig. 6*j*,*k*). Like NAT10, SYT9 is predominantly expressed in β-Tubulin III-

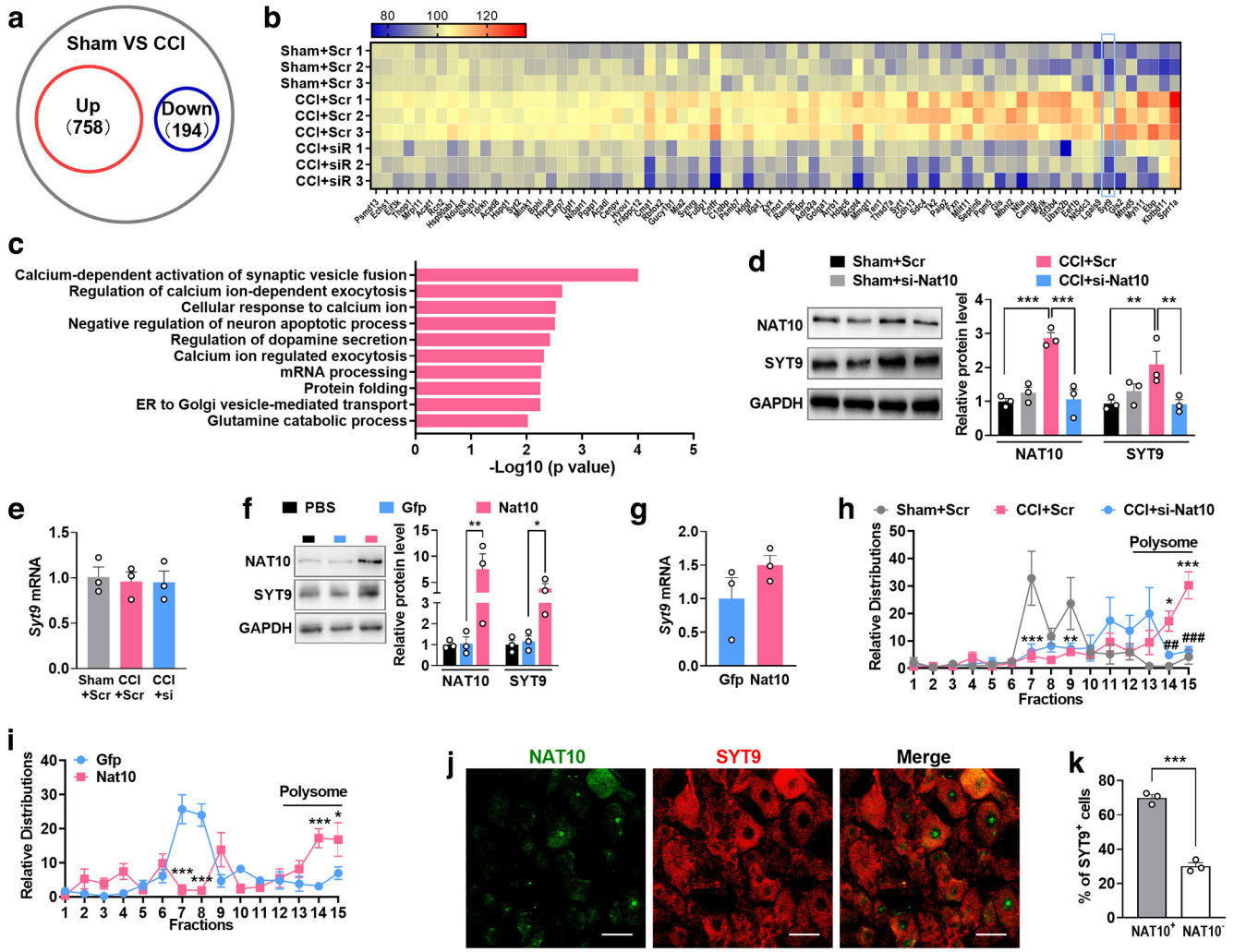

Figure 6. NAT10 upregulation is required for the CCI-induced increase in SYT9 expression in injured DRG. ***a***, Analysis of protein expression profiles in the ipsilateral L3/4 DRGs on day 7 after CCI, compared with the sham group. Differentially expressed proteins were filtered to $p < 0.05$ and abundance >1.2-fold change. There were 758 upregulated proteins and 194 downregulated proteins. ***b***, Heatmap showing that upregulation of the 74 proteins in the ipsilateral L3/4 DRGs in CCI mice was reversed by NAT10 knock-down on day 3 after microinjection of *Nat10* siRNA (siR) or scrambled siRNA (Scr). $n = 8$ mice/sample, each group had three independent samples. 1, 2, and 3 represent the sample number in each group. High expression is indicated by reddish colors and low expression by blueish colors. The protein outlined in light blue is SYT9. ***c***, The top 10 biological processes of these 74 proteins, as indicated by analysis of the Gene Ontology database. ***d***, ***e***, The level of SYT9 protein (***d***) and mRNA (***e***) on day 3 after microinjection of *Nat10* siRNA (si-*Nat10*) or scrambled siRNA (Scr) into L3/4 DRGs 7 d after CCI or sham surgery. $n = 6$ mice/group, $^{**}p < 0.01$, $^{***}p < 0.001$ versus the corresponding groups; two-way ANOVA, *post hoc* Tukey's test. ***f***, ***g***, The level of SYT9 protein (***f***) and *Syt9* mRNA (***g***) on day 6 after microinjection of Lenti-*Nat10* (Nat10) or Lenti-*Gfp* (Gfp) into L3/4 DRG of naive mice. $n = 6$ mice/group, $^{*}p < 0.05$, $^{**}p < 0.01$ versus Gfp control; two-way ANOVA, *post hoc* Tukey's test. ***h***, Polysome assay showing the translation state of *Syt9* mRNA in the ipsilateral L3/4 DRGs 3 d after microinjection with *Nat10* siRNA (si-*Nat10*) or scrambled siRNA (Scr) in mice subjected to CCI or sham surgery. $n = 24$ mice/group; $^{*}p < 0.05$, $^{**}p < 0.01$, $^{***}p < 0.001$ versus the sham-plus-Scr group; $^{\#\#}p < 0.01$, $^{\#\#\#}p < 0.001$ versus the CCI-plus-Scr group; two-way ANOVA, *post hoc* Tukey's test. ***i***, The translation state of *Syt9* mRNA 6 d after microinjection of Lenti-*Nat10* (Nat10) or Lenti-*Gfp* (Gfp) into L3/4 DRGs of naive mice. $n = 24$ mice/group, $^{*}p < 0.05$, $^{***}p < 0.001$ versus Gfp control; two-way ANOVA, *post hoc* Tukey's test. ***j***, Co-expression of SYT9 (red) with NAT10 (green) in individual DRG cells. Scale bar, 30 μm. ***k***, Histogram showing the percentage of SYT9-positive cells that were also positive for NAT10. Almost 70% SYT9-positive cells co-expressed NAT10. $n = 6$ mice/group, $^{***}p < 0.001$ versus the percentage of SYT9-positive cells that were negative for NAT10. See Extended Data Figure 6-1.

positive cells in the DRG but not GS-positive satellite cells, indicating a neuronal locus (Extended Data Fig. 6-1*c*,*d*). Subcellular analysis showed that SYT9 was located predominantly in the cytoplasm of DRG neurons (Extended Data Fig. 6-1*e*). Finally, we cultured adult DRG neurons to carry out the single-cell PCR experiment to analyze the co-expression of SYT9, NAT10, and USF1 in DRG neurons. The results showed that SYT9, NAT10, and USF1 co-existed in individual small, medium, and large DRG neurons (Extended Data Fig. 6-1*f*–*h*). Overall, these data demonstrate that SYT9 is functionally coupled to NAT10, likely in a posttranscription-dependent manner.

Gain-of-ac4C in the *Syt9* mRNA gene coding domain sequence mediates the NAT10-controlled increase in SYT9 protein in the DRG of CCI mice

We next sought to establish whether Syt9 mRNA can be acetylated and whether SYT9 protein expression is regulated by the ac4C modification. As ac4C occurs frequently in specific repeated "CXXCXXCXX" motifs ("X" represents A, G, C, or U) in mRNA, especially in the gene coding domain sequence (CDS; Arango et al., 2018). Using the specific motifs, we identified six regions may be containing the ac4C motif (Fig. 7*a*). Four pairs of primers were designed to cover all of the predicted motif regions [PCR primer pair 1 for the a (+79 to

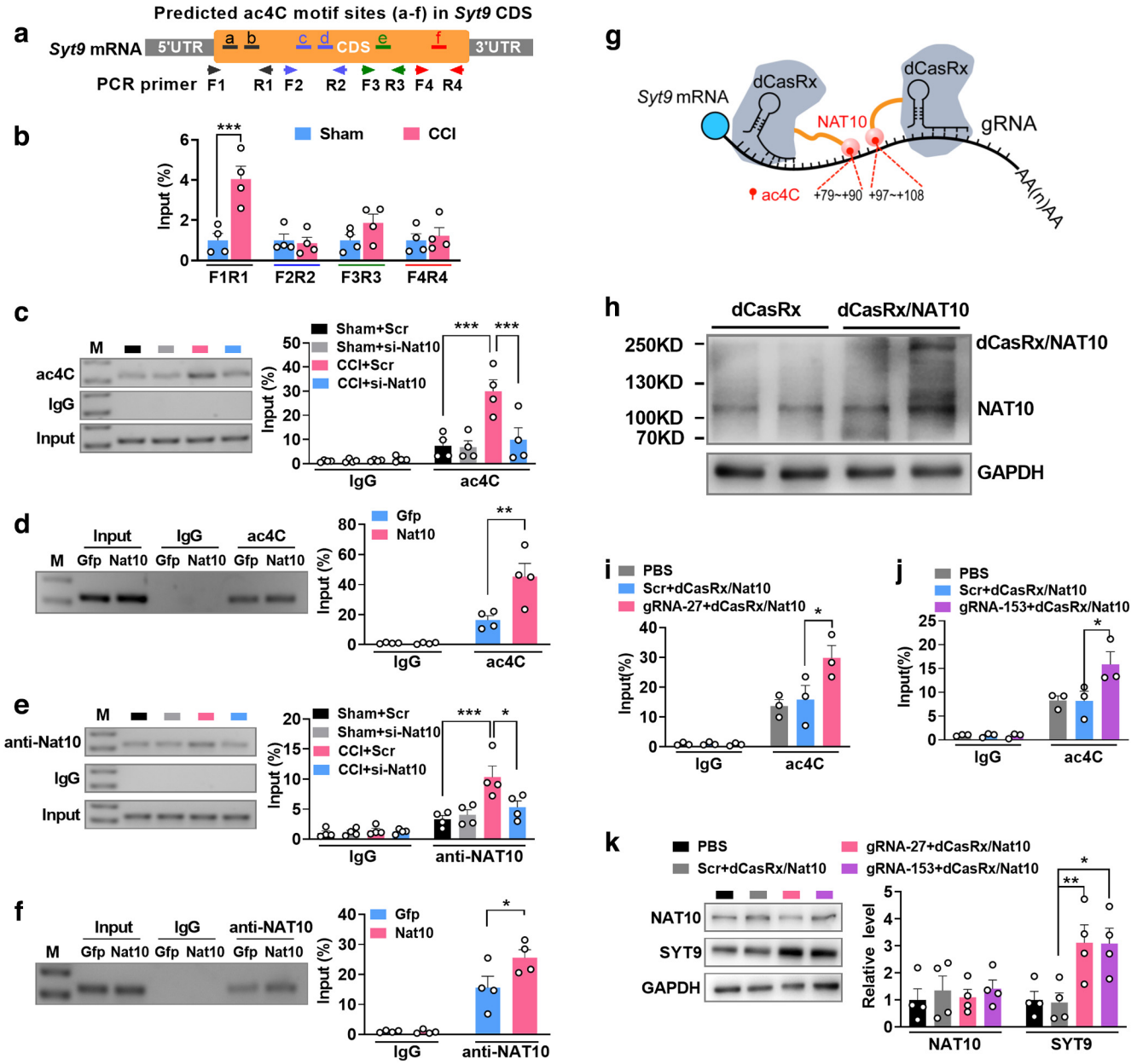

Figure 7. Elevated ac4C in *Syt9* mRNA mediates the NAT10-triggered increase in SYT9 protein after CCI. ***a***, The predicted ac4C motif (CXXCXXCXX. X represents A, G, C, or U) location in the CDS of *Syt9* mRNA. The forward and reverse arrows represent paired RT-PCR primers. a-f, the six ac4C motif regions in the *Syt9* CDS. F and R, The designed PCR primer pairs for amplifying the specific ac4C motifs. ***b***, Detection of the six corresponding ac4C motifs via RNA immunoprecipitation (RIP)-PCR using the four PCR primer pairs. $n = 9$ mice/group, $^{***}p < 0.001$ versus the sham group; two-way ANOVA, *post hoc* Tukey's test. ***c***, RIP-PCR with anti-ac4C revealed the ac4C level of *Syt9* CDS (a and b motif sites) on 3 d after microinjection of *Nat10*-siRNA (siRNA) or scrambled siRNA (Scr) into L3/4 DRGs of CCI or Sham mice with 7 d surgery. $n = 12$ mice/group, $^{***}p < 0.001$ versus the corresponding groups; two-way ANOVA, *post hoc* Tukey's test. ***d***, ac4C level of *Syt9* on 5 d after microinjection of Lenti-*Nat10* or Lenti-*Gfp* into L3/4 DRGs of naive mice. $n = 12$ mice/group, $^{**}p < 0.01$ versus Gfp control; two-way ANOVA, *post hoc* Tukey's test. ***e***, Lanti-*Nat10* antibody revealed the binding accounts of NAT10 to *Syt9* CDS after microinjection of *Nat10*-siRNA (siRNA) or scrambled siRNA (Scr) into L3/4 DRGs of CCI or Sham mice with 7 d surgery. $n = 12$ mice/group, $^{*}p < 0.05$, $^{***}p < 0.001$ versus the corresponding groups; two-way ANOVA, *post hoc* Tukey's test. ***f***, The binding accounts of NAT10 to *Syt9* CDS on 5 d after microinjection of Lenti-*Nat10* or Lenti-*Gfp* of naive mice. $n = 12$ mice/group, $^{*}p < 0.05$ versus the corresponding groups; two-way ANOVA, *post hoc* Tukey's test. ***g***, CRISPR-dCasRx "writing" ac4C to the given CDS in *Syt9* mRNA. gRNA, small guide RNA. +79 to +90 and +97 to +108 represent the locations of the a and b ac4C motif sites in the *Syt9* CDS. The first nucleotide of the CDS is designated as +1. ***h***, Identification of dCasRx-NAT10 fusion protein expression on day 5 after microinjection of CRISPR-dCasRx-Nat10 into L3/4 DRGs. ***i***, ***j***, Analysis of ac4C levels in the *Syt9* CDS on day 5 after co-microinjection of CRISPR-dCasRx-Nat10 and gRNA-27 or gRNA-153 into L3/4 DRGs in naive mice. $n = 6$ mice/group, $^{*}p < 0.05$ versus the corresponding groups; two-way ANOVA, *post hoc* Tukey's test. gRNA-27 (+27 to +46, first nucleotide in the CDS is designated as +1) and gRNA-153 (+153 to +172) were designed to bind to near the a and b sites in the *Syt9* CDS. ***k***, The expression level of SYT9 and NAT10 on day 5 after co-microinjection of CRISPR-dCasRx-Nat10 and gRNA-27 or gRNA-153 into unilateral L3/4 DRGs in naive mice. $n = 8$ mice/group, $^{*}p < 0.05$, $^{**}p < 0.01$ versus the corresponding groups; two-way ANOVA, *post hoc* Tukey's test.

+90) and b (+97 to +108) motifs, pair 2 for the c (+973 to +987) and d (+991 to +1002) motifs, pair three for the e (+1108 to +1119) motif, and pair four for the f (+1270 to +1281) motif, with the first nucleotide of the CDS designated as +1] (Fig. 7*a*). An RNA immunoprecipitation (RIP) assay revealed that the two CDS fragments containing the a/b or e motifs (but not the fragments containing the c, d, or f motifs) could be amplified from the sham DRG complex immunoprecipitated with the ac4C antibody (Fig. 7*b*). CCI increased the ac4C level in the a/b motif by 300%, but did

not significantly affect ac4C in the e motif; microinjection of Nat10-siRNA returned the ac4C increase in the a/b motif almost to the basal level on day 3 after microinjection, but the scrambled control did not (Fig. 7*c*).

NAT10 upregulation by Lenti-Nat10 enhanced the ac4C level in the a/b motif by 176% in the injected DRG, compared with the Lenti-Gfp control (Fig. 7*d*). Given that NAT10 serves as a "writer," adding ac4C onto mRNA, we measured the binding level of NAT10 to a/b motif regions under the modulation conditions described above. Like ac4C in the a/b motif, microinjection of Nat10-siRNA not the scrambled control reversed the increased NAT10 binding to the a/b motif in the L3/4 DRGs of CCI mice on day 3 postinjection (Fig. 7*e*). Microinjection of Lenti-Nat10, but not Lenti-Gfp, elevated the NAT10 binding level in the DRG of naive mice on day 6 postinjection (Fig. 7*f*). Thus, NAT10 likely participates in the regulation of ac4C modification of Syt9 mRNA.

We next used the CRISPR gene-editing system (Lorsch et al., 2019) to further confirm the specific regulatory role of ac4C in SYT9 protein expression. NAT10 was fused with inactivated CasRx protein (dCasRx/NAT10 fusion protein) to specifically "write" ac4C to the a/b motif via guide RNA (gRNA; Fig. 7*g*). The dCasRx/NAT10 fusion protein was detectable on day 5 after microinjection of lentivirus CRISPR-dCasRx-Nat10 in naive mice (Fig. 7*h*). Two gRNAs including gRNA-27 (+27 to +46, first nucleotide in the CDS designated as +1) and gRNA-153 (+153 to +172) located near the a/b motif were designed as previous described (Hofacker et al., 2020). Syt9 ac4C levels in CCI DRGs were increased by 72.2% and 132% versus the Scr group on day 5 after co-microinjection of CRISPR-dCasRx-Nat10 and gRNA-27 or gRNA-153, respectively (Fig. 7*i*,*j*). Furthermore, co-microinjection of CRISPR-dCasRx-Nat10 with gRNA-27 or gRNA-153, not the Scr gRNA, co- significantly enhanced the level of SYT9 expression in the DRGs by 305% and 283% on day 5 post-CCI (Fig. 7*k*). These manipulations did not impair normal locomotor functions (Table 2). Taken together, these data show that nerve-injury-induced SYT9 upregulation is required for CCI-evoked ac4C elevation via NAT10 in injured DRGs.

NAT10 regulates SYT9 under nociceptive conditions

We next asked whether NAT10 regulates neuropathic pain via modulation of SYT9. First, we examined the effect of DRG SYT9 on neuropathic pain behavior. DRG microinjection of Syt9-siRNA on day 7 post-CCI not only decreased SYT9 expression (Fig. 8*a*), but also alleviated mechanical allodynia and heat hyperalgesia on days 10 and 13 post-CCI on the ipsilateral side (Fig. 8*b*–*d*). As expected, the basal paw responses on the contralateral side (Extended Data Fig. 8-1*a*–*c*) and locomotor behavior (Table 2) were not affected in these mice. Overexpression by microinjection of lentivirus with full-length Syt9 caused a significantly increased expression of SYT9 in L3/4 DRGs of naive mice (Fig. 8*e*). This overexpression induced nociceptive hypersensitivity starting from day 4 after microinjection in L3/4 DRGs of naive mice (Fig. 8*f*–*h*). Similarly, SYT9 upregulation by microinjection of CRISPR-dCasRx-Nat10 and gRNA-27 or gRNA-153 also induced mechanical and thermal pain hypersensitivity from days 6 to 10 after microinjection (Fig. 8*i*–*k*). No impairments in locomotor function were seen in these mice (Table 2). These findings suggest that SYT9 regulates neuropathic pain. Finally, we confirmed the relationship between NAT10 and SYT9 and their role in neuropathic pain. Microinjection of Syt9-siRNA not only reduced the increase of SYT9 protein caused by overexpression of NAT10 (Fig. 8*l*), but also blocked the pain hypersensitivity which was induced by DRG microinjection of Lenti-*Nat10* though co-microinjection of Lenti-Nat10 and Syt9-siRNA (Fig. 8*m*–*o*). Collectively, our data identify NAT10 as a key initiator in neuropathic pain that acts at least partly by targeting SYT9 in an ac4C-dependent manner (Fig. 9).

Discussion

Recent studies have shown extensive N4-acetylcytidine (ac4C) modifications in mammalian mRNA (Arango et al., 2018). ac4C is emerging a novel regulatory mechanism that improves the translation efficiency and stability of mRNA, and it has drawn widespread attention for its vital roles in various biological processes and human diseases (Arango et al., 2018, 2022). Significant changes in ac4C content are detectable in the serum, plasma or urine of patients with gestational diabetes (Jin et al., 2020), myocardial infarction (K. Wang et al., 2022b), interstitial cystitis (Parsons et al., 2014), acquired immunodeficiency syndrome (AIDS; Tsai et al., 2020), cancer (Szymańska et al., 2010; T. Zhang et al., 2013; H. Li et al., 2019), chronic renal failure, relapsed refractory cirrhosis (Bhargava et al., 2019), and pulmonary fibrosis (Laguna et al., 2015). In addition, oxidative stress significantly increased the ac4C content in yeast mRNA (Tardu et al., 2019). Despite this, the potential role of ac4C in pain has remained unknown. Here, we identified an increase in ac4C in injured DRGs and found that this increase could be attributed to upregulation of NAT10 in DRG neurons after peripheral nerve injury. Furthermore, we demonstrated that the USF1-controlled NAT10 upregulation initiated and maintained neuropathic pain through increased ac4C-triggered SYT9 translation efficiency in DRG neurons. NAT10 therefore appears to play a key role in nerve injury-induced pain hypersensitivity in an ac4C-dependent manner.

Like other pain-related genes, Nat10 can be regulated at the transcriptional level. Peripheral nerve injury caused an increase in NAT10 expression at least in part through nerve-injury-induced upregulation of USF1 and subsequent gain of its binding to the Nat10 gene promoter in injured DRG (Fig. 2*c*). Additionally, NAT10 and USF1 are co-expressed in all types of DRG neurons. This is consistent with previous findings showing that USF1 is ubiquitously expressed in neurons in peripheral and central nerve tissues (Chen et al., 2003; Park and Russo, 2008; Zhou et al., 2022). Indeed, USF1 belongs to the family of basic helix–loop–helix leucine zipper (bHLH-LZ)-type transcription factors. USF1 can recognize and bind the "CACGTG" motif in the gene-promoter regions alone or in cooperation with other transcription factors like USF2 (Costa et al., 2020). Because of the existence of the "CACGTG" in the Nat10 promoter, USF1 binds to the Nat10 promoter and regulates Nat10 transcription (Fig. 2*d*,*e*). Interestingly, USF1 is known to regulate Ca^{2+}-dependent gene transcription in the nervous system and could thus control neuronal-activity-regulated genes such as Cox-2, Nur77, nAchRa7, and GAP-43 (Chen et al., 2003), as well as the Fmr1, Bdnf, and App genes (Kumari and Usdin, 2001; Chen et al., 2003; Hu et al., 2017). Functionally, mice lacking USF1 display spontaneous epilepsy (Sirito et al., 1998), suggesting that USF1 may play a key role in nervous system diseases. More importantly for the study of pain, we demonstrated that blocking DRG USF1 not only reversed the CCI-induced upregulation of NAT10 expression but also reversed the nerve-injury-induced nociceptive hypersensitivity. In naive mice, DRG overexpression of USF1 increased NAT10 expression and enhanced responses to nociceptive stimuli. Our findings establish that the role of USF1 in neuropathic pain is at least partly through targeting of DRG NAT10. Whether

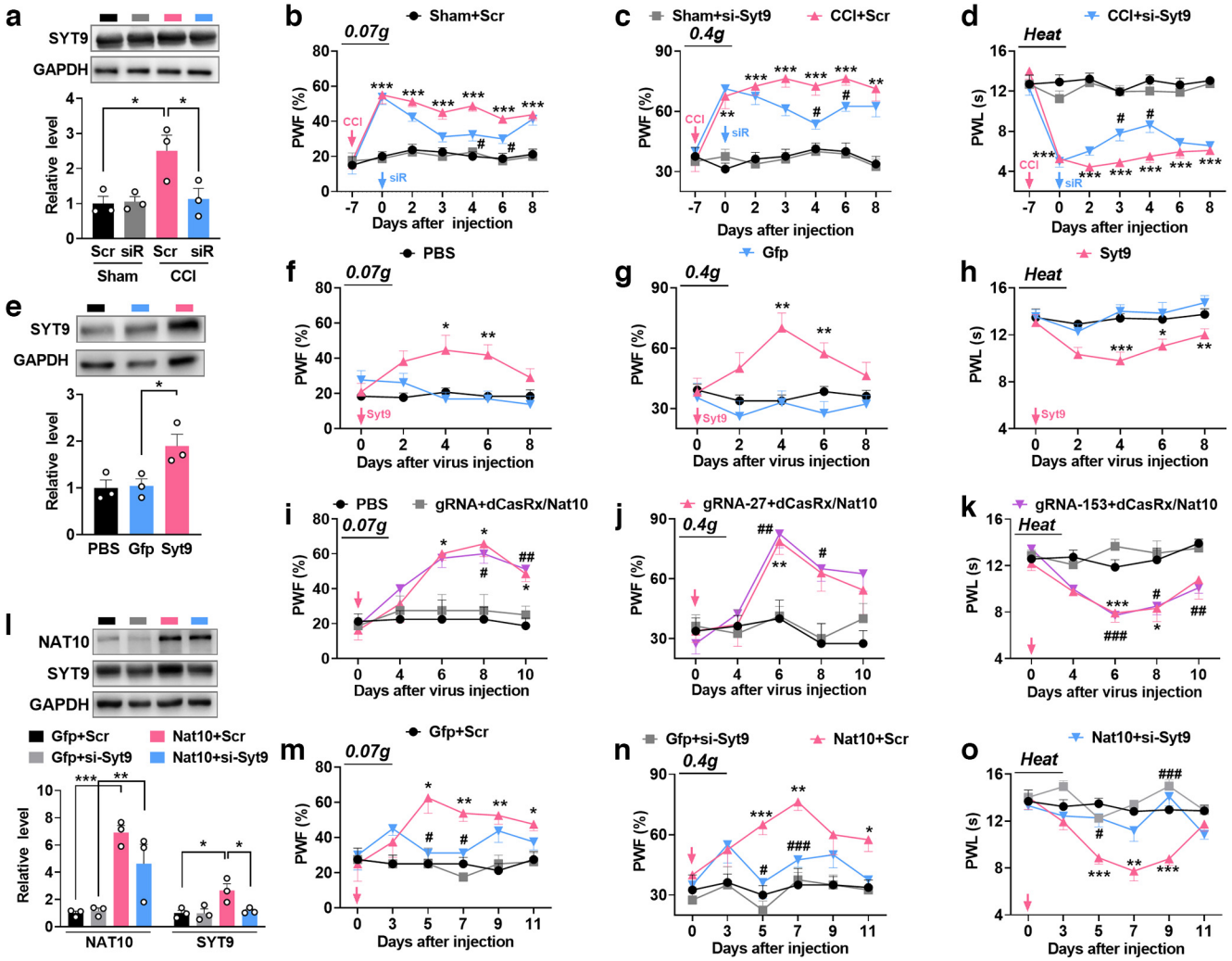

Figure 8. SYT9 mediates the regulatory effect of NAT10 on neuropathic pain. ***a***, The level of SYT9 protein 3 d after DRG microinjection of *Syt9*-siRNA (siR) or scrambled siRNA (Scr) into L3/4 DRGs CCI mice 7 d postsurgery. $n = 6$ mice/group, $^{*}p < 0.05$ versus the corresponding groups; one-way ANOVA, *post hoc* Tukey's test. ***b–d***, Effect of microinjection of *Syt9* siRNA (si-*Syt9*) and scrambled siRNA (Scr) into the ipsilateral L3/4 DRGs on the development of CCI-induced mechanical allodynia (***b***, ***c***) and heat hyperalgesia (***d***) on the ipsilateral side. $n = 8$ mice/group, $^{**}p < 0.01$ and $^{***}p < 0.001$ versus the sham-plus-Scr group; $\#p < 0.05$ versus CCI-plus-Scr group; two-way ANOVA, *post hoc* Tukey's test. ***e,*** DRG SYT9 protein levels 4 d after microinjection of Lenti-*Syt9* into L3/4 DRGs of naive mice. $n = 6$ mice/group, $^{*}p < 0.05$ versus Gfp; one-way ANOVA, *post hoc* Tukey's test. ***f–h***, Time course of the effect of microinjection of Lenti-*Syt9* (Syt9) or Lenti-*Gfp* (Gfp) into the unilateral L3/4 DRGs on the ipsilateral nociceptive response to 0.07 g (***f***) and 0.4 g (***g***) von Frey filaments and to heat stimuli (***h***). $n = 8$ mice/group, $^{*}p < 0.05$, $^{**}p < 0.01$, and $^{***}p < 0.001$ versus Gfp group; two-way ANOVA, *post hoc* Tukey's test. ***i–k***, Effect of co-microinjection of CRISPR-dCasRx-Nat10 and gRNA-27 or gRNA-153 into unilateral L3/4 DRGs on the paw-withdrawal frequencies to 0.07 g (***i***) and 0.4 g (***j***) von Frey filaments and to heat stimuli (***k***). $n = 8$ mice/group, $^{*}p < 0.05$, $^{**}p < 0.01$, $^{***}p < 0.001$, the gRNA-27-plus-CRISPR-dCasRx-Nat10 group versus the scrambled gRNA (gRNA)-plus-CRISPR-dCasRx-Nat10 group; $\#p < 0.05$, $\#\#p < 0.01$, $\#\#\#p < 0.001$, the gRNA-153-plus-CRISPR-dCasRx-Nat10 versus the gRNA-plus-CRISPR-dCasRx-Nat10; two-way ANOVA, *post hoc* Tukey's test. ***l***, Protein levels of NAT10 and SYT9 in the DRGs on day 5 after co-microinjection of Lenti-*Nat10* (or Lenti-*Gfp*) and *Syt9*-siRNA (or scrambled siRNA) in naive mice. $n = 6$ mice/group, $^{*}p < 0.05$, $^{**}p < 0.01$, $^{***}p < 0.001$ versus the corresponding groups; two-way ANOVA, *post hoc* Tukey's test. ***m–o***, Time course of the effect of knocking down *Syt9* with siRNA on the development of neuropathic-pain-like behavior induced by *Nat10* upregulation by Lenti-*Nat10*. Lenti-*Nat10* (or Lenti-*Gfp*) and *Syt9*-siRNA (or scrambled siRNA) were co-microinjected into the unilateral L3/4 DRGs of naive mice. $n = 8$ mice/group, $^{*}p < 0.05$, $^{**}p < 0.01$, $^{***}p < 0.001$ versus the Lenti-*Gfp*-plus-Scr group; $\#p < 0.05$, $\#\#\#p < 0.001$ versus the Lenti-*Nat10*-plus-Scr; two-way ANOVA, *post hoc* Tukey's test. See Extended Data Figure 8-1.

other transcription factors also participate in NAT10 upregulation in injured DRG is unclear. A recent study has shown that the lysine residue at 426 (K426) in NAT10 protein is acetylated, resulting in enhancement of NAT10 activity (Cai et al., 2017). Therefore, the observed increase in DRG NAT10 in our study might also result from posttranscriptional modification or other epigenetic modifications. These possibilities cannot be ruled out and will be addressed in future studies.

NAT10 can catalyze ac4C after recognizing the ac4C motif in mRNA and has served as an important player in the development of various diseases (Arango et al., 2018; G. Wang et al., 2022a). In the present study, our data support the conclusion that the nerve-injury-induced increase in DRG NAT10 is required for the induction and maintenance of neuropathic pain. Notably, knocking down DRG NAT10 via microinjection of Nat10-siRNA or shRNA in wild-type mice, or via microinjection of AAV2-Cre in $Nat10^{fl/fl}$ mice, markedly blocked the CCI-induced increase in the overall ac4C level in the DRG, resulting in the suppression of NAT10 expression levels in injured DRG and the abolishment of neuropathic pain. However, NAT10 reduction was not observed in sham DRG after siRNA or shRNA injection. The possible reason is that DRG is a complex tissue, this characteristic may give it a strong compensatory metabolic capacity to protect itself against the injury under the physiological status. Thus, after injection of Nat10-siRNAs into Sham DRG, the defensive

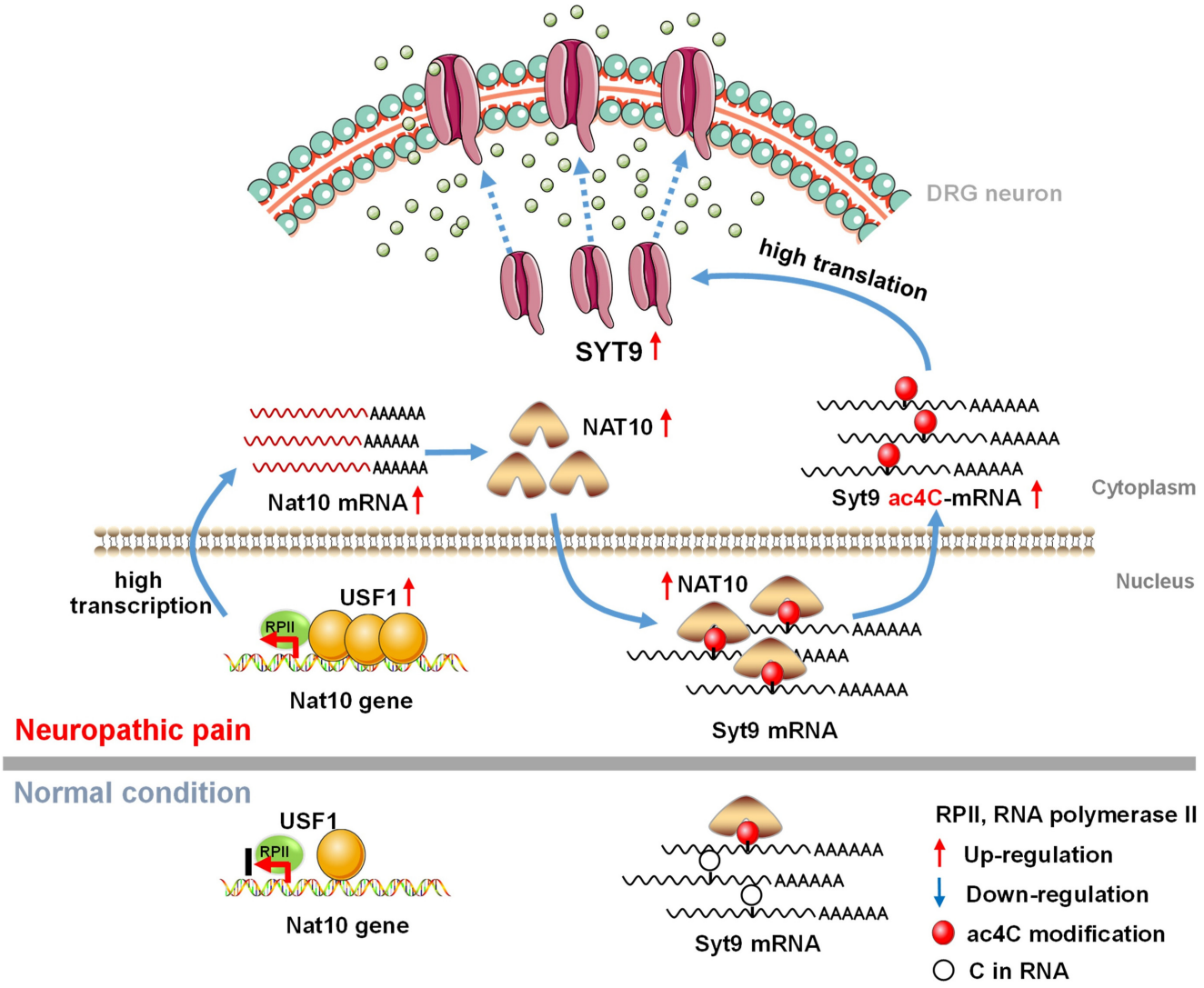

Figure 9. The schematic shows that the cytidine N-Acetyltransferase NAT10 participates in peripheral nerve injury-induced neuropathic pain by stabilizing SYT9 expression in primary sensory neurons. Peripheral nerve injury upregulates NAT10 level in the injured DRGs. This upregulation is attributed to an increase in the binding accounts of USF1 to *Nat10 promoter* in DRGs neurons. Furthermore, the upregulated NAT10 elevates the level of ac4C in *Syt9* CDS, triggering in the increase of SYT9 protein expression and genesis of nociceptive hypersensitivity.

proteins could almost completely or mostly degrade these exogenous molecules, so as to, to a large degree, protect Nat10 mRNA. In fact, in the similar experiments of other pain research groups, they also find the consistent phenomena, in which siRNAs do not or less affect the expression of the target genes (J. Zhang et al., 2016; S. Wang et al., 2019; Du et al., 2022). Moreover, this knock-down in the DRG of CCI mice abolished CCI-induced hyperactivation in dorsal horn neurons and astrocytes. Mimicking nerve-injury-induced NAT10 upregulation with DRG microinjection of Lenti-Nat10 in naive mice caused an increase in the overall ac4C level in the DRG and augmented the animals' response to noxious stimuli. This DRG NAT10 upregulation in *naive* mice also induced hyperactivation of dorsal horn neurons and astrocytes. Previous studies have shown that ac4C contributes to the production of nascent proteins by improving the stability and translation efficiency of mRNA (Arango et al., 2018). Here, we found that the level of nascent protein is positively correlated with NAT10 abundance in the DRG, suggesting that NAT10 improves translation efficiency by controlling the overall level of ac4C in DRG. To our knowledge, this is the first evidence that NAT10 contributes to neuropathic pain in an ac4C-dependent manner.

NAT10 upregulation caused an increase in the level of SYT9 protein, but not mRNA, in the DRG following nerve injury. We found that blocking NAT10 significantly reversed this SYT9 increase, demonstrated by an unbiased protein mass-spectrometry profile. SYT9 is one member of the synaptotagmin family, which contributes to Ca^{2+}-dependent neurotransmitter release (Fernandez-Chacon et al., 2001). It is well documented that other members of the synaptotagmin family, such as SYT1 and SYT2, are involved in the endogenous initiation of neuropathic pain through their role in neurotransmitter release (Alvarado et al., 2015; Wan et al., 2020) but the role of SYT9 has not been established. Therefore, from the candidate proteins, we selected SYT9 as the putative downstream target of NAT10. We observed that SYT9 was mainly located in neurons in the DRG, and was co-expressed with NAT10. At the molecular level, we found six ac4C motif sites as the described previously (Arango et al., 2018; G. Wang et al., 2022a). Of these, the +79 to +90 and +97 to +108 sites were identified as regulated by NAT10 in the DRG post-CCI. There are currently no agonists or inhibitors of ac4C

activity available so we used the CRISPR-dCasRx system to confirm a direct relationship between ac4C and SYT9 protein expression. We constructed a specific fusion protein containing NAT10 and dCasRx, in which the NAT10 protein was placed precisely at the ac4C motifs by guide gRNA that recognized a given ac4C site sequence in the Syt9 CDS. Upregulating the level of the two ac4C motifs resulted not only in an increase in SYT9, but also in the production of neuropathic-pain-like behavior. Overexpressing DRG SYT9 by microinjected full-length Syt9 lentivirus produced a consistent nociceptive phenomenon in naive mice, and blocking the increased SYT9 in the DRG significantly relieved the nerve-injury- or NAT10-upregulation-induced pain hypersensitivity. It is clear that SYT9 is a critical regulator of neuropathic pain; whether the involvement of SYT9 in neuropathic pain depends on Ca^{2+}-dependent neurotransmitter release will be investigated in future studies. Additionally, although SYT9 is expressed in both male and female anterior pituitary cells, SYT9 is involved in the modulation of follicle-stimulating hormone secretion in a female-specific manner (Roper et al., 2015). Given that only male mice were used in the present study, whether the mechanisms discussed above are male-specific is unknown.

Interestingly, we found the robust effects of Nat10 on mechanical than on thermal hypersensitivity. This difference may be attributed to the existence of one or more other unknown downstream genes of NAT10, which may be more sensitive to mechanical pain, or more insensitive to thermal pain. In fact, except for the sharing sensory signal molecules, mechanical pain and thermal pain own their individual specific sensory signal molecules. For example, TRPV1 and TRPM3, enriched in sensory neurons, are the noxious heat sensor and are required for the development of heat hyperalgesia (Vriens et al., 2011; Vandewauw et al., 2018; Tanimizu et al., 2021). Whereas, TACAN, a recently identified ion channel, mainly contributes to sensing mechanical pain (Beaulieu-Laroche et al., 2020).

In summary, we demonstrated that nerve injury increases the level of NAT10 expression and the overall ac4C level in injured DRGs. Reversing this abnormal increase relieves pain hypersensitivity without affecting basal responses or locomotor function in a Syt9-ac4C-dependent manner. This is the first time that RNA ac4C modification has been linked to neuropathic pain: this relationship may provide a new therapeutic avenue in ongoing search for effective treatments for neuropathic pain. Our results suggest that NAT10 may be a key target for the management of neuropathic pain.

References

Alsaloum M, Waxman SG (2022) iPSCs and DRGs: stepping stones to new pain therapies. Trends Mol Med 28:110–122.

Alvarado S, Tajerian M, Suderman M, Machnes Z, Pierfelice S, Millecamps M, Stone LS, Szyf M (2015) An epigenetic hypothesis for the genomic memory of pain. Front Cell Neurosci 9:88.

Arango D, Sturgill D, Alhusaini N, Dillman AA, Sweet TJ, Hanson G, Hosogane M, Sinclair WR, Nanan KK, Mandler MD, Fox SD, Zengeya TT, Andresson T, Meier JL, Coller J, Oberdoerffer S (2018) Acetylation of cytidine in mRNA promotes translation efficiency. Cell 175:1872–1886.e24.

Arango D, Sturgill D, Yang R, Kanai T, Bauer P, Roy J, Wang Z, Hosogane M, Schiffers S, Oberdoerffer S (2022) Direct epitranscriptomic regulation of mammalian translation initiation through N4-acetylcytidine. Mol Cell 82:2797–2814.e11.

Bao BY, Pao JB, Huang CN, Pu YS, Chang TY, Lan YH, Lu TL, Lee HZ, Juang SH, Chen LM, Hsieh CJ, Huang SP (2011) Polymorphisms inside microRNAs and microRNA target sites predict clinical outcomes in prostate cancer patients receiving androgen-deprivation therapy. Clin Cancer Res 17:928–936.

Beaulieu-Laroche L, et al. (2020) TACAN is an ion channel involved in sensing mechanical pain. Cell 180:956–967.e17.

Bhargava P, Fitzgerald KC, Venkata SLV, Smith MD, Kornberg MD, Mowry EM, Haughey NJ, Calabresi PA (2019) Dimethyl fumarate treatment induces lipid metabolism alterations that are linked to immunological changes. Ann Clin Transl Neurol 6:33–45.

Cai S, Liu X, Zhang C, Xing B, Du X (2017) Autoacetylation of NAT10 is critical for its function in rRNA transcription activation. Biochem Biophys Res Commun 483:624–629.

Cavalli E, Mammana S, Nicoletti F, Bramanti P, Mazzon E (2019) The neuropathic pain: an overview of the current treatment and future therapeutic approaches. Int J Immunopathol Pharmacol 33:2058738419838383.

Chen WG, West AE, Tao X, Corfas G, Szentirmay MN, Sawadogo M, Vinson C, Greenberg ME (2003) Upstream stimulatory factors are mediators of Ca2+-responsive transcription in neurons. J Neurosci 23:2572–2581.

Costa L, Corre S, Michel V, Le Luel K, Fernandes J, Ziveri J, Jouvion G, Danckaert A, Mouchet N, Da Silva Barreira D, Torres J, Camorlinga M, D'Elios MM, Fiette L, De Reuse H, Galibert MD, Touati E (2020) USF1 defect drives p53 degradation during Helicobacter pylori infection and accelerates gastric carcinogenesis. Gut 69:1582–1591.

Du S, Wu S, Feng X, Wang B, Xia S, Liang L, Zhang L, Govindarajalu G, Bunk A, Kadakia F, Mao Q, Guo X, Zhao H, Berkman T, Liu T, Li H, Stillman J, Bekker A, Davidson S, Tao YX (2022) A nerve injury-specific long noncoding RNA promotes neuropathic pain by increasing Ccl2 expression. J Clin Invest 132:e153563.

Fernandez-Chacon R, Konigstorfer A, Gerber SH, Garcia J, Matos MF, Stevens CF, Brose N, Rizo J, Rosenmund C, Sudhof TC (2001) Synaptotagmin I functions as a calcium regulator of release probability. Nature 410:41–49.

Friedrich C, Schallenberg S, Kirchner M, Ziehm M, Niquet S, Haji M, Beier C, Neudecker J, Klauschen F, Mertins P (2021) Comprehensive micro-scaled proteome and phosphoproteome characterization of archived retrospective cancer repositories. Nat Commun 12:3576.

Gautam V, D'Avanzo C, Berezovska O, Tanzi RE, Kovacs DM (2015) Synaptotagmins interact with APP and promote Abeta generation. Mol Neurodegener 10:31.

Geppert M, Goda Y, Hammer RE, Li C, Rosahl TW, Stevens CF, Sudhof TC (1994) Synaptotagmin I: a major Ca2+ sensor for transmitter release at a central synapse. Cell 79:717–727.

Guo XF, Wang XH, Fu YL, Meng Q, Huang BY, Yang R, Guo Y, Du YR, Wang X, Gao Y, Song L, Gong M, Wang S, Li YD, Shi HS, Shi Y (2022) Elevation of N-acetyltransferase 10 in hippocampal neurons mediates depression- and anxiety-like behaviors. Brain Res Bull 185:91–98.

Hofacker D, Broche J, Laistner L, Adam S, Bashtrykov P, Jeltsch A (2020) Engineering of effector domains for targeted DNA methylation with reduced off-target effects. Int J Mol Sci 21:502.

Hu XT, Zhu BL, Zhao LG, Wang JW, Liu L, Lai YJ, He L, Deng XJ, Chen GJ (2017) Histone deacetylase inhibitor apicidin increases expression of the α-secretase ADAM10 through transcription factor USF1-mediated mechanisms. FASEB J 31:1482–1493.

Jin G, Xu M, Zou M, Duan S (2020) The processing, gene regulation, biological functions, and clinical relevance of N4-acetylcytidine on RNA: a systematic review. Mol Ther Nucleic Acids 20:13–24.

Kumari D, Usdin K (2001) Interaction of the transcription factors USF1, USF2, and alpha -Pal/Nrf-1 with the FMR1 promoter. Implications for Fragile X mental retardation syndrome. J Biol Chem 276:4357–4364.

Laguna TA, Reilly CS, Williams CB, Welchlin C, Wendt CH (2015) Metabolomics analysis identifies novel plasma biomarkers of cystic fibrosis pulmonary exacerbation. Pediatr Pulmonol 50:869–877.

Larrieu D, Britton S, Demir M, Rodriguez R, Jackson SP (2014) Chemical inhibition of NAT10 corrects defects of laminopathic cells. Science 344:527–532.

Li H, Qin Q, Shi X, He J, Xu G (2019) Modified metabolites mapping by liquid chromatography-high resolution mass spectrometry using full scan/all ion fragmentation/neutral loss acquisition. J Chromatogr A 1583:80–87.

Li J, Chen Z, Chen F, Xie G, Ling Y, Peng Y, Lin Y, Luo N, Chiang CM, Wang H (2020) Targeted mRNA demethylation using an engineered dCas13b-ALKBH5 fusion protein. Nucleic Acids Res 48:5684–5694.

Li Y, Guo X, Sun L, Xiao J, Su S, Du S, Li Z, Wu S, Liu W, Mo K, Xia S, Chang YJ, Denis D, Tao YX (2020) N(6)-methyladenosine demethylase

FTO contributes to neuropathic pain by stabilizing G9a expression in primary sensory neurons. Adv Sci (Weinh) 7:1902402.
Liang P, Hu R, Liu Z, Miao M, Jiang H, Li C (2020) NAT10 upregulation indicates a poor prognosis in acute myeloid leukemia. Curr Probl Cancer 44:100491.
Liu XS, Zhou LM, Yuan LL, Gao Y, Kui XY, Liu XY, Pei ZJ (2021) NPM1 is a prognostic biomarker involved in immune infiltration of lung adenocarcinoma and associated with m6A modification and glycolysis. Front Immunol 12:724741.
Lorsch ZS, et al. (2019) Stress resilience is promoted by a Zfp189-driven transcriptional network in prefrontal cortex. Nat Neurosci 22:1413–1423.
Ma H, Tu LC, Naseri A, Huisman M, Zhang S, Grunwald D, Pederson T (2016) Multiplexed labeling of genomic loci with dCas9 and engineered sgRNAs using CRISPRainbow. Nat Biotechnol 34:528–530.
Mongelli A, Atlante S, Bachetti T, Martelli F, Farsetti A, Gaetano C (2020) Epigenetic signaling and RNA regulation in cardiovascular diseases. Int J Mol Sci 21:509.
Pan Z, Zhang M, Ma T, Xue ZY, Li GF, Hao LY, Zhu LJ, Li YQ, Ding HL, Cao JL (2016) Hydroxymethylation of microRNA-365-3p regulates nociceptive behaviors via Kcnh2. J Neurosci 36:2769–2781.
Pan Z, Xue ZY, Li GF, Sun ML, Zhang M, Hao LY, Tang QQ, Zhu LJ, Cao JL (2017) DNA hydroxymethylation by ten-eleven translocation methylcytosine dioxygenase 1 and 3 regulates nociceptive sensitization in a chronic inflammatory pain model. Anesthesiology 127:147–163.
Pan Z, Li GF, Sun ML, Xie L, Liu D, Zhang Q, Yang XX, Xia S, Liu X, Zhou H, Xue ZY, Zhang M, Hao LY, Zhu LJ, Cao JL (2019) MicroRNA-1224 splicing circularRNA-Filip1l in an Ago2-dependent manner regulates chronic inflammatory pain via targeting Ubr5. J Neurosci 39:2125–2143.
Pan Z, Zhang Q, Liu X, Zhou H, Jin T, Hao LY, Xie L, Zhang M, Yang XX, Sun ML, Xue ZY, Tao Y, Ye XC, Shen W, Cao JL (2021a) Methyltransferase-like 3 contributes to inflammatory pain by targeting TET1 in YTHDF2-dependent manner. Pain 162:1960–1976.
Pan Z, Du S, Wang K, Guo X, Mao Q, Feng X, Huang L, Wu S, Hou B, Chang YJ, Liu T, Chen T, Li H, Bachmann T, Bekker A, Hu H, Tao YX (2021b) Downregulation of a dorsal root ganglion-specifically enriched long noncoding RNA is required for neuropathic pain by negatively regulating RALY-triggered Ehmt2 expression. Adv Sci (Weinh) 8:e2004515.
Panda AC, Martindale JL, Gorospe M (2017) Polysome fractionation to analyze mRNA distribution profiles. Bio Protoc 7:e2126.
Park KY, Russo AF (2008) Control of the calcitonin gene-related peptide enhancer by upstream stimulatory factor in trigeminal ganglion neurons. J Biol Chem 283:5441–5451.
Parsons CL, Shaw T, Berecz Z, Su Y, Zupkas P, Argade S (2014) Role of urinary cations in the aetiology of bladder symptoms and interstitial cystitis. BJU Int 114:286–293.
Pasero C (2004) Pathophysiology of neuropathic pain. Pain Manag Nurs 5:3–8.
Rigaud M, Gemes G, Barabas ME, Chernoff DI, Abram SE, Stucky CL, Hogan QH (2008) Species and strain differences in rodent sciatic nerve anatomy: implications for studies of neuropathic pain. Pain 136:188–201.
Roper LK, Briguglio JS, Evans CS, Jackson MB, Chapman ER (2015) Sex-specific regulation of follicle-stimulating hormone secretion by synaptotagmin 9. Nat Commun 6:8645.
Schmidt EK, Clavarino G, Ceppi M, Pierre P (2009) SUnSET, a nonradioactive method to monitor protein synthesis. Nat Methods 6:275–277.
Sirito M, Lin Q, Deng JM, Behringer RR, Sawadogo M (1998) Overlapping roles and asymmetrical cross-regulation of the USF proteins in mice. Proc Natl Acad Sci U S A 95:3758–3763.
Szymańska E, Markuszewski MJ, Markuszewski M, Kaliszan R (2010) Altered levels of nucleoside metabolite profiles in urogenital tract cancer measured by capillary electrophoresis. J Pharm Biomed Anal 53:1305–1312.
Tan TZ, Miow QH, Huang RY, Wong MK, Ye J, Lau JA, Wu MC, Bin Abdul Hadi LH, Soong R, Choolani M, Davidson B, Nesland JM, Wang LZ, Matsumura N, Mandai M, Konishi I, Goh BC, Chang JT, Thiery JP, Mori S (2013) Functional genomics identifies five distinct molecular subtypes with clinical relevance and pathways for growth control in epithelial ovarian cancer. EMBO Mol Med 5:1051–1066.
Tanimizu N, Ichinohe N, Sasaki Y, Itoh T, Sudo R, Yamaguchi T, Katsuda T, Ninomiya T, Tokino T, Ochiya T, Miyajima A, Mitaka T (2021) Generation of functional liver organoids on combining hepatocytes and cholangiocytes with hepatobiliary connections ex vivo. Nat Commun 12:3390.
Tardu M, Jones JD, Kennedy RT, Lin Q, Koutmou KS (2019) Identification and quantification of modified nucleosides in *Saccharomyces cerevisiae* mRNAs. ACS Chem Biol 14:1403–1409.
Teng PC, Liang Y, Yarmishyn AA, Hsiao YJ, Lin TY, Lin TW, Teng YC, Yang YP, Wang ML, Chien CS, Luo YH, Chen YM, Hsu PK, Chiou SH, Chien Y (2021) RNA modifications and epigenetics in modulation of lung cancer and pulmonary diseases. Int J Mol Sci 22:10592.
Tsai K, Jaguva Vasudevan AA, Martinez Campos C, Emery A, Swanstrom R, Cullen BR (2020) Acetylation of cytidine residues boosts HIV-1 gene expression by increasing viral RNA stability. Cell Host Microbe 28:306–312.e6.
Tschida BR, Temiz NA, Kuka TP, Lee LA, Riordan JD, Tierrablanca CA, Hullsiek R, Wagner S, Hudson WA, Linden MA, Amin K, Beckmann PJ, Heuer RA, Sarver AL, Yang JD, Roberts LR, Nadeau JH, Dupuy AJ, Keng VW, Largaespada DA (2017) Sleeping beauty insertional mutagenesis in mice identifies drivers of steatosis-associated hepatic tumors. Cancer Res 77:6576–6588.
Vandewauw I, De Clercq K, Mulier M, Held K, Pinto S, Van Ranst N, Segal A, Voet T, Vennekens R, Zimmermann K, Vriens J, Voets T (2018) A TRP channel trio mediates acute noxious heat sensing. Nature 555:662–666.
van Hecke O, Austin SK, Khan RA, Smith BH, Torrance N (2014) Neuropathic pain in the general population: a systematic review of epidemiological studies. Pain 155:654–662.
Vriens J, Owsianik G, Hofmann T, Philipp SE, Stab J, Chen X, Benoit M, Xue F, Janssens A, Kerselaers S, Oberwinkler J, Vennekens R, Gudermann T, Nilius B, Voets T (2011) TRPM3 is a nociceptor channel involved in the detection of noxious heat. Neuron 70:482–494.
Wan J, Nan S, Liu J, Ding M, Zhu H, Suo C, Wang Z, Hu M, Wang D, Ding Y (2020) Synaptotagmin 1 is involved in neuropathic pain and electroacupuncture-mediated analgesic effect. Int J Mol Sci 21:968.
Wang G, Zhang M, Zhang Y, Xie Y, Zou J, Zhong J, Zheng Z, Zhou X, Zheng Y, Chen B, Liu C (2022a) NAT10-mediated mRNA N4-acetylcytidine modification promotes bladder cancer progression. Clin Transl Med 12:e738.
Wang K, Zhou LY, Liu F, Lin L, Ju J, Tian PC, Liu CY, Li XM, Chen XZ, Wang T, Wang F, Wang SC, Zhang J, Zhang YH, Tian JW, Wang K (2022b) PIWI-interacting RNA HAAPIR regulates cardiomyocyte death after myocardial infarction by promoting NAT10-mediated ac(4) C acetylation of Tfec mRNA. Adv Sci (Weinh) 9:e2106058.
Wang S, Liu S, Xu L, Zhu X, Liu W, Tian L, Chen Y, Wang Y, Nagendra BVP, Jia S, Liang L, Huo FQ (2019) The upregulation of EGFR in the dorsal root ganglion contributes to chronic compression of dorsal root ganglions-induced neuropathic pain in rats. Mol Pain 15:174480691985729.
Wang Y, Jones-Tabah J, Chakravarty P, Stewart A, Muotri A, Laposa RR, Svejstrup JQ (2016) Pharmacological bypass of Cockayne syndrome B function in neuronal differentiation. Cell Rep 14:2554–2561.
Wang Y, Shi Y, Huang Y, Liu W, Cai G, Huang S, Zeng Y, Ren S, Zhan H, Wu W (2020) Resveratrol mediates mechanical allodynia through modulating inflammatory response via the TREM2-autophagy axis in SNI rat model. J Neuroinflammation 17:311.
Wolfes AC, Dean C (2020) The diversity of synaptotagmin isoforms. Curr Opin Neurobiol 63:198–209.
Yang MF, Long XX, Hu HS, Bin YL, Chen XM, Wu BH, Peng QZ, Wang LS, Yao J, Li DF (2021) Comprehensive analysis on the expression profile and prognostic values of synaptotagmins (SYTs) family members and their methylation levels in gastric cancer. Bioengineered 12:3550–3565.
Ye F, Wang T, Wu X, Liang J, Li J, Sheng W (2021) N6-methyladenosine RNA modification in cerebrospinal fluid as a novel potential diagnostic biomarker for progressive multiple sclerosis. J Transl Med 19:316.
Yi MH, Liu YU, Liu K, Chen T, Bosco DB, Zheng J, Xie M, Zhou L, Qu W, Wu LJ (2021) Chemogenetic manipulation of microglia inhibits neuroinflammation and neuropathic pain in mice. Brain Behav Immun 92:78–89.
Zeng K, He B, Yang BB, Xu T, Chen X, Xu M, Liu X, Sun H, Pan Y, Wang S (2018) The pro-metastasis effect of circANKS1B in breast cancer. Mol Cancer 17:160.

Zhang H, Hou W, Wang HL, Liu HJ, Jia XY, Zheng XZ, Zou YX, Li X, Hou L, McNutt MA, Zhang B (2014) GSK-3β-regulated N-acetyltransferase 10 is involved in colorectal cancer invasion. Clin Cancer Res 20:4717–4729.

Zhang J, Liang L, Miao X, Wu S, Cao J, Tao B, Mao Q, Mo K, Xiong M, Lutz BM, Bekker A, Tao YX (2016) Contribution of the suppressor of variegation 3-9 homolog 1 in dorsal root ganglia and spinal cord dorsal horn to nerve injury-induced nociceptive hypersensitivity. Anesthesiology 125:765–778.

Zhang T, Wu X, Ke C, Yin M, Li Z, Fan L, Zhang W, Zhang H, Zhao F, Zhou X, Lou G, Li K (2013) Identification of potential biomarkers for ovarian cancer by urinary metabolomic profiling. J Proteome Res 12:505–512.

Zhang Y, Jing Y, Wang Y, Tang J, Zhu X, Jin WL, Wang Y, Yuan W, Li X, Li X (2021) NAT10 promotes gastric cancer metastasis via N4-acetylated COL5A1. Signal Transduct Target Ther 6:173.

Zhao H, Chen Q, Li F, Cui L, Xie L, Huang Q, Liang X, Zhou J, Yan X, Zhu X (2021) Fibrogranular materials function as organizers to ensure the fidelity of multiciliary assembly. Nat Commun 12:1273.

Zhao JY, Liang L, Gu X, Li Z, Wu S, Sun L, Atianjoh FE, Feng J, Mo K, Jia S, Lutz BM, Bekker A, Nestler EJ, Tao YX (2017) DNA methyltransferase DNMT3a contributes to neuropathic pain by repressing Kcna2 in primary afferent neurons. Nat Commun 8:14712.

Zhao X, Tang Z, Zhang H, Atianjoh FE, Zhao JY, Liang L, Wang W, Guan X, Kao SC, Tiwari V, Gao YJ, Hoffman PN, Cui H, Li M, Dong X, Tao YX (2013) A long noncoding RNA contributes to neuropathic pain by silencing Kcna2 in primary afferent neurons. Nat Neurosci 16:1024–1031.

Zhou Y, Meng X, He W, Li X, Zhao R, Dong C, Yuan D, Yang J, Zhang R, Shi G, Huang Y, Liu J, Liu J, Liu S, Fu P, Sun M (2022) USF1/CD90 signaling in maintaining glioblastoma stem cells and tumor-associated macrophages adhesion. Neuro Oncol 24:1482–1493.